UNIVERSITY OF FORWARD THINKING WESTMINSTER

Poly(3-hydroxyoctanoate), a promising new material for cardiac tissue engineering

Bagdadi, A., Safari, M., Dubey, P., Basnett, P., Sofokleous P., Humphrey E, Locke, I.C., Edirisinghe M., Terracciano C., Boccaccini, A.R., Knowles, J.C., Harding, S. and Roy, I.

This is the peer reviewed version of the following article: Bagdadi, A., Safari, M., Dubey, P., Basnett, P., Sofokleous P., Humphrey E, Locke, I.C., Edirisinghe M., Terracciano C., Boccaccini, A.R., Knowles, J.C., Harding, S. and Roy, I. (2016) Poly(3-hydroxyoctanoate), a promising new material for cardiac tissue engineering, *Journal of Tissue Engineering and Regenerative Medicine*, doi: 10.1002/term.2318, which has been published in final form at:

https://dx.doi.org/10.1002/term.2318

Poly(3-hydroxyoctanoate), a promising new material for cardiac tissue engineering

Andrea V. Bagdadi [1], Maryam Safari [1], Prachi Dubey [1], Pooja Basnett [1], Panagiotis Sofokleous [2], Eleanor Humphrey [6], Ian Locke [1] , Mohan Edirisinghe[2] , Cesare Terracciano[6], Aldo R. Boccaccini [3] , Jonathan C. Knowles[4,5], Sian E. Harding [6], Ipsita Roy [1]*

1. Applied Biotechnology Research Group, Faculty of Science and Technology, University of Westminster, London, UK
2. Department of Mechanical Engineering, UCL, London, UK
3. Department of Materials Science and Engineering, University of Erlangen-Nuremberg, Erlangen, Germany
4. Department of Biomaterials and Tissue engineering, Eastman Dental Institute, UCL, London, UK
5. Department of Nanobiomedical Science & BK21 Plus NBM Global Research Center for Regenerative Medicine, Dankook University, Republic of Korea
6. National Heart and Lung Institute, Imperial College, London, UK

*Corresponding author

Professor Ipsita Roy

Faculty of Science and Technology

University of Westminster

115 New Cavendish Street

London W1W 6UW, UK

Abstract:

Cardiac tissue engineering (CTE) is currently a prime focus of research due to an enormous clinical need. In this work, a novel functional material, Poly(3-hydroxyoctanoate), P(3HO), a medium chain length polyhydroxyalkanoate (PHA), produced using bacterial fermentation, was studied as a new potential material for CTE. Engineered constructs with improved mechanical properties, crucial for supporting the organ during new tissue regeneration, and enhanced surface topography, to allow efficient cell adhesion and proliferation, were fabricated. Our results showed that the mechanical properties of the final patches were close to that of cardiac muscle. Biocompatibility of the P(3HO) neat patches, assessed using Neonatal ventricular rat myocytes (NVRM), showed that the polymer was as good as collagen in terms of cell viability, proliferation and adhesion. Enhanced cell adhesion and proliferation properties were observed when porous and fibrous structures were incorporated to the patches. Also, no deleterious effect was observed on the adults cardiomyocytes' contraction when cardiomyocytes were seeded on the P(3HO) patches. Hence, P(3HO) based multifunctional cardiac patches are promising constructs for efficient CTE. This work will provide a positive impact on the development of P(3HO) and other PHAs as a novel new family of biodegradable functional materials with huge potential in a range of different biomedical applications, particularly CTE, leading to further interest and exploitation of these materials.

Keywords: Cardiac Tissue Engineering, Polyhydroxyalkanoates, Poly(3-hydroxyoctanoate), cardiac patches

1. Introduction

Cardiovascular diseases (CVDs) are the leading cause of death throughout the world (Morosco 2002, Perry and Roth 2003). According to the World Health Organization, an estimated 17.3 million people died from CVDs in 2008 and it is predicted that by 2030 almost 25 million people will die from CVDs. Myocardial infarction is the main cause of death in patients with CVDs. The acute loss of myocardium triggers a cascade of cell signals activating a ventricular and early and late remodelling process. The early ventricular remodelling process includes the formation, thinning and elongation of a fibrotic scar that cause elevation of diastolic and systolic wall stresses. An increased wall stress leads to a late remodelling characterized by myocyte hypertrophy and production of interstitial collagen with an increased wall mass and chamber enlargement (Sutton and Shape 2000). Myocardial infarction may eventually lead to the deterioration of systolic or diastolic function and to increased predisposition to arrhythmias and other long-term complications.

The combination of a natural or synthetic biomaterial with relevant cells and growth factors *ex vivo* is currently receiving much attention for cardiac tissue engineering treatments (Giraud *et al.*, 2007). The final goal will be the selection of an appropriate cell type and the development of a biocompatible flexible functional material that stimulates cell growth and guides and supports tissue regeneration in order to replace the formed scar tissue with functioning cardiac muscle tissue. The material's physical and mechanical characteristics should be similar enough to those of the natural myocardium in order to support the organ during the regeneration process, and its composition should allow it to degrade as the new tissue is formed (Jawad *et al.*, 2008). Bioabsorbable polymeric materials provide an extracellular matrix where growing cells can localize and interact to form new tissue. An ideal biomaterial should possess five special characteristics. First, the material should be biocompatible. Second, the

material's mechanical properties should be similar to the host tissue to provide mechanical support to the cells until the cells synthesize new extracellular matrix. As previously described, myocardial infarction normally results in wall thinning and ventricular dilatation that causes a significant stress in the heart wall. An overstressed wall leads to a progressive ventricular remodelling with an end stage of heart failure (Sutton and Shape 2000). In order to prevent an overstressed wall with a negative ventricular remodelling, the material's mechanical properties should allow reduction of the heart wall stress (Chen *et al.,* 2008). Third, the material should possess an appropriate shape and size to guide and organize the cells and to repair at the implant site. Fourth, the chemistry of the material's surface should allow cell attachment, differentiation and proliferation. Fifth, the composition of the material should allow biodegradation *in vivo* at rates appropriate for tissue regeneration (Williams *et al.,* 1999).

In this work we propose Poly(3-hydroxyoctanoate), P(3HO), a medium chain length biodegradable and biocompatible polyhydroxyalkanoate, as a novel functional healthcare material for application in CTE to deliver cells to the injured tissue and to support the heart during its regeneration process. PHAs are polyesters composed of several units of hydroxyalkanoate monomers linked to each other through ester linkages. Numerous microorganisms synthesize PHAs by the fermentation of a carbon source and then accumulate them as intracellular carbon reserve inclusion bodies. Previous literature has shown that *Pseudomonas mendocina* produced a unique P(3HO) homopolymer when sodium octanoate was used as a sole carbon source with an excess supply of carbon and limitation of nitrogen (Rai *et al.,* 2011). The P(3HO) homopolymer is a unique candidate for cardiac tissue engineering due to its biocompatibility, biodegradability and elastomeric properties. One of the main reasons

of PHA biocompatibility is the presence of some PHA monomer units in human blood and tissues (Hocking *et al.*, 1994, Nelson *et al.*, 1981). Additionally, PHA biodegradation occurs by erosion from the surface to the interior in contrast to other amorphous polymers such as PLGA, which exhibit bulk degradation (Weng *et al.*, 2011). Finally, the combination of P(3HO)'s low crystallinity (37.5%), with Tg values below ambient temperature, imparts to the polymer an elastomeric behaviour crucial to support the organ for synchronised beating (Rai *et al.*, 2011).

Collagen, as the main constituent of the myocardial extracellular matrix, facilitates cell adhesion and proliferation and maintain cells in their differentiated states because of its particular adhesive properties (Jawad *et al.*, 2008). In this work, in order to understand the P(3HO) biocompatibility and adhesive properties, freshly isolated NVRMs were seeded on both P(3HO) and collagen, and the cell viability was compared.

An appropriate level of cardiomyocyte contraction is a crucial factor for a highly regulated mechanical system such as the heart, in order to maintain its accurate pumping function. The effect of the P(3HO) polymer on contracting cardiomyocytes was studied by seeding freshly isolated adult cardiomyocytes from rat on P(3HO) patches films.

Engineered P(3HO) cardiac patches with appropriate mechanical properties to support the injured organ and to allow cell growth for efficient cell delivery were created. Our first approach was the design of permeable porous structures with pore size comparable to that of cardiomyocytes, with an appropriate surface structure for cell attachment, which permits the ingress of cells and guides their growth, leading to tissue regeneration in three dimensions. Eventually, the polymer matrix would be degraded leaving behind new tissue. In a second approach, as collagen is the main constituent of the extracellular matrix and exhibits a distinct fibrous architecture, in order to mimic such fibrous

structure, the neat P(3HO) and porous patch surfaces were modified using optimal electrospun P(3HO) fibres with sizes selected according to the highest cell affinity and proliferation observed. P(3HO) fibres were deposited on neat and porous P(3HO) films. *In vitro* cell culture work using C2C12 myoblast cell line was carried out to assess the final cardiac patches.

Finally, as the contractile nature of the cardiac tissue demands readily available high oxygen and nutrient concentrations, delivery of angiogenic growth factors from the engineered graft is a key factor to encourage the rapid development of the vascular network. For this, the vascular endothelial growth factor (VEGF) was incorporated in to the patches and VEGF release was studied over 30 days. In addition, for an enhanced interaction of the construct with cells, the arginine-glycine-aspartic tripeptide sequence (RGD peptide) was immobilized on the patch surface.

2. Materials and Methods

2.1. P(3HO) production

P. mendocina was used for the production of poly-3-hydroxyoctanoate, a mcl-PHA. The polymer production and extraction and purification were carried out as previously described (Rai *et al*., 2011). The P(3HO) homopolymer was extracted using the method involving the dispersion of chloroform and sodium hypochlorite.

2.2. P(3HO) characterization

The structural characterization of the obtained polymer was carried out by Fourier transform infrared spectroscopy (FTIR), Gas Chromatography-Mass spectroscopy (GC-MS) and Nuclear magnetic resonance (NMR).

2.2.1. Fourier transform infrared spectroscopy (FTIR)

FTIR analysis was carried out to determine the presence of the PHA functional groups in the sample. A Perkin Elmer series 2000 FTIR spectrometer with a spectral range 4000 to 400 cm-1 was used at the Department of Biomaterials and Tissue Engineering, Eastman Dental Institute, University College London, UK. For both, the whole cell analysis and extracted PHA polymer, 2 mg of lyophilised cells or polymer were used.

2.2.2. Gas Chromatography-Mass spectroscopy (GC-MS)

The monomer content of the extracted PHA was identified by GC-MS. Before the analysis, the polymer was methanolysed as previously described (Wang *et al.*, 2006). For this, 15 mg of polymer were added to 1 ml of the esterification solution containing 3 ml of 95–98% H2SO4, 0.29 g of methylbenzoate, and 97 ml of methanol. Then, 1 ml of chloroform was added and the mixture was heated at 100 °C for 4 hr. After the 4 hours, the mixture was cooled and 1 ml of MiliQ water was added and vortexed for phase separation. The lower phase was extracted, dried over anhydrous Na2SO4, neutralized by Na2CO3 and filtered (Wang *et al*., 2006). The analysis was carried out using a Trace2000 GC–MS (Thermo, San Jose, USA) containing a ZB-5MS (Phenomenex, Torrance, CA, USA) column (30 m length, 0.25 mm-internal diameter, and 0.25 μm-film thickness). The sample (1 μL), in chloroform, was injected, with helium (1 mL min−1) as the carrier gas. The injector temperature was 220 ˚C and the column temperature was increased from 40 to 320 ˚C at 20 ˚C min^{-1} and held at the final temperature for 6 min.

2.2.3. Nuclear magnetic resonance (NMR)

The extracted PHA monomer structure was confirmed by NMR. The analysis was carried out on 30 mg of polymer dissolved in 1 mL of the deuterated chloroform

($CDCl_3$). The 1H and 13C spectra were obtained in a Bruker® AV400 (400 MHz) spectrometer at the Chemistry Department, University College London, UK.

2.3. Neat and porous P(3HO) cardiac patches fabrication

The plain and porous films fabrication was carried out by the solvent cast technology. For this, 0.5 g of P(3HO) were dissolved in 10 ml of chloroform and poured on 60 mm diameter glass petri dishes. Porous structures were incorporated by the Solvent Casting Particle Leaching (SCPL) technique. In this case, 50 mg of sucrose particles between 250 and 300 μm of size, selected using molecular sieves, were added to the dissolved polymer before casting. The polymer was dried at the ambient temperature (20°C-25°C) for 7 days and then freeze dried for 10 days.

2.4. Neat and porous cardiac patches functionalization with P(3HO) fibrous structures

The electrospinning technique was used for the fabrication of P(3HO) microfibres. For this, the following P(3HO) solutions were produced in acetone: 0.2 wt%, 0.5 wt%, 0.6 wt%, 0.7 wt%, 1 wt% and 1.2 wt%. A syringe was loaded with the polymer solution and pumped by a Harvard® syringe pump through silicone tubing connected to a nozzle. The conductive steel nozzle was connected to a positive terminal of a Glassman Europe® high voltage supply source. The electric potential and the pump speed were adjusted for each concentration until a stable jetting was obtained. For the optimization of the electrospinning conditions, two sizes of inner diameter nozzles (330μm and 660μm) were tested at a range of flow rates (from 30 μl/min to 250 μl/min). A stable jetting and homogeneous fibres were obtained when the 330 μm needle and 30 μl/min flow rate were used and the electric potential was adjusted. Higher electric potentials were required with lower polymer concentrations. The electric potential used for the

1.2 wt%, 1 wt%, 0.7 wt%, 0.6 wt%, 0.5 wt% and 0.2 wt% polymer solution were 8.9, 10.9, 11.4, 11.6 13.4 and 13.8, kV respectively. A distance of 150 mm between the needle and collector was used in all conditions tested. A range of collection times were assessed in each condition (from 1 to 90 seconds) and one collection time was selected in each case. The fibre collection was carried out on plain and porous P(3HO) films and glass slides.

2.5. P(3HO) cardiac patch characterization

The physical properties of the material were determined by Dynamic mechanical analysis (DMA), Differential scanning calorimetry (DSC) and the surface properties were analysed by contact angle analysis, profilometry and scanning electron microscopy (SEM).

2.5.1. Dynamic mechanical analysis (DMA)

The mechanical properties of the polymer were analysed using a Perkin–Elmer®dynamic mechanical analyser. The analysis was carried out under static conditions on polymer strips of 10 mm length and 4 mm width. The initial load was set to 1 mN and then increased to 6000 mN at the rate of 200 mN min^{-1} and the stress and strain were measured. The Young's modulus, tensile strength and elongation at break were calculated from the stress vs. strain plot. The experiment was repeated after polymer strips were incubated in PBS at 37 °C for two hours.

2.5.2. Differential scanning calorimetry (DSC)

The thermal properties of the polymer were determined using a Perkin Elmer®Pyris Diamond DSC. For the analysis, approximately 8 mg of sample were placed in aluminium pans and the samples were cooled down to -57 ºC. Then, samples were heated, cooled and heated again at a heating rate of 20 ºC min-1 from -57 ºC to 175 ºC,

and the glass transition temperature (Tg), melting temperature (Tm) and crystallization temperature (Tc) were determined.

2.5.3. Contact angle analysis

The water contact angle of the fabricated films was analysed on a KSV Cam 200® optical contact angle. For this, a Hamilton® syringe was loaded with MiliQ water and a drop of water was dispensed on the film. A series of photos were taken every second to record the shape of the drop over 20 seconds. The water contact angle was measured using a KSVCam® software.

2.5.4. Surface roughness analysis

Surface roughness studies were carried out on a UBM laser scanning profilometer. An area of 2 mm x 2 mm (± 500 μm) was scanned by the machine in two directions. A graphical representation of the scans and average roughness values were recorded.

2.5.5. Scanning electron microscopy (SEM)

The surface of the films was examined under a JEOL 5410LV Scanning electron microscope (Hertfordshire, UK). The samples were placed on Agar Scientific® Carbon conducting tabs and then coated with gold-palladium using a Quorum Technologies® Polaron E5000 Sputter Coater (East Sussex, UK) for 2 minutes. The SEM images were taken with an acceleration voltage of 10 kV at 150 mm working distance.

2.5.6. Porosity measurements

The porosity of the films was determined using equation (1).

$$\text{Porosity (\%)} = \frac{Vm - Vp}{Vm} \times 100 = \frac{Vm - (W\rho/\rho)}{Vm} \times 100 \qquad (1)$$

where Vm is the volume of the plain films, Vρ is the volume of the porous film, and Wρ, ρ and ρ is the mass and density of the porous film, respectively. Porosity measurements were made in quadruplicates.

2.5.7. Fibre measurements

The size and shape of the fibres obtained by electrospinning was assessed by optical microscopy. Image tool® software was used to measure the size of the fibres. An average of the fibres size was calculated in each condition from the measurement of 30 fibres.

2.6. Cardiomyocyte compatibility studies

2.6.1. Cardiomyocyte viability

In vitro biocompatibility studies were performed using freshly isolated Neonatal ventricular rat myocytes (NVRM). P(3HO) patches were cut in to 1 cm^2 squares, placed on a 12 well plate and sterilized using UV light for 30 minutes on each side. The NRVMs were seeded on the P(3HO) patches and collagen coated slices, used as control, in NRVM medium: 67% Dulbecco's modified Eagle medium (DMEM), 16% Medium 199, 10% Horse serum (HS) (Gibco), 4% foetal bovine serum (FBS) (Gibco), 2% HEPES (4-(2-hydroxyethyl)-1-piperazineethanesulfonic acid) buffer and 1% penicillin-streptomycin. Live/dead assay was conducted on day 2 for the NVRM cells grown on P(3HO) and collagen. A live/ dead cell cytotoxicity assay was used to label the cells. Cells were washed in sterile PBS and 100 μL of 2 μM calcein AM and 4 μM ethidium homodimer-1 solution was added to each well for 30 min in the dark, at room temperature. Following incubation, the samples were mounted in fresh PBS and imaged using an inverted Zeiss LSM-780 confocal microscope. Cells were counted using the

Fiji image processing software (ImageJ). The study was carried out in triplicates for each sample.

2.6.1.1. Immunofluorescence

NVRM cells seeded on P(3HO) cardiac patches were washed in phosphate buffered saline (PBS), fixed with ice-cold methanol for 5 min and blocked in 1% bovine serum albumin (BSA) (subsequently used for all antibody dilutions) for 1 hour. Cells were stained with a primary antibody mouse anti- α actinin antibody (1:1000 dilution) (sigma) overnight at 4°C and then incubated with a secondary antibody anti-mouse Cy3 antibody (1:500 dilution) (Millipore) for 1 hour at room temperature before mounting in vectashield (Vectalabs) mounting medium containing DAPI. The cells were imaged using an inverted Zeiss LSM-780 confocal microscope.

2.6.2.Cardiomyocyte contraction

Fresh adult rat beating cardiomyocytes were seeded on a P(3HO) coated cover slip. The cardiomyocytes were superfused at 37°C in modified Krebs-Henseleit solution: NaCl 118.5mM, KCl 5.9mM, $NaHCO_3$ 25mM, $MgSO_4$ 1.2mM, NaH_2PO_4 1.38mM, Glucose 11mM, 1 mM $CaCl_2$, buffered with 95%O2/5%CO_2, and delivered at 36-37°C, pH 7.4. For the study, rod shaped cardiomyocytes with regular contraction under electrical stimulation, and no spontaneous contraction without stimulation, were selected. Cells were stimulated with pulses of 50 V for 2 ms with 2 second intervals. Contraction amplitude (% shortening), 'time to peak 90 %' and 'time to relaxation 50 %' were recorded with an IonOptix® video based system. The myocyte contraction was studied at a range of frequencies of electrical pulses of 50 V for a period of 2 ms. Starting from 2 second interval pulses, the intervals were increased to 5 seconds, and then decreased to 2 seconds, 1 second and 0.5 seconds. Following this, the effect of the

calcium increment was studied. With a 2 second interval pulse of 2 ms at 50 V, the $CaCl_2$ concentration of the solution was increased from 1 mM to 2 mM, and then 3 mM and 4 mM. A stabilization period of at least 5 min was allowed in each condition. The contraction studies were also carried out on uncoated cover slips as controls. The contraction experiments were carried out on preparations from 4 animals.

2.7. P(3HO) functionalization with active molecules

2.7.1. Human vascular endothelial growth factor (VEGF) incorporation within the P(3HO) film

The VEGF film fabrication was carried out by dissolving 0.5 g of the P(3HO) polymer in 10 ml of chloroform. Then, 2 µl of a 1 µg/µl human VEGF solution in MiliQ water were added into the polymer solution. The resulting solution was vortexed for 5 minutes and cast in 60 mm Petri dishes. Films were dried at 4 ºC for 21 days.

VEGF release kinetics from P(3HO) patches:

The *in vitro* VEGF release from films was studied for 30 days (Sipahigil *et al.,* 2012). In this experiment 10 mg of films were incubated in Eppendorf tubes containing 1 ml of PBS at 37 ºC with constant agitation at 100 rpm. 500 µl of PBS were periodically withdrawn from the tubes and replaced with fresh PBS at the following time points (days): 1, 3, 5, 7, 10, 13, 17, 21, 25 and 30. The amount of VEGF released in the medium was measured using the Invitrogen®VEGF human ELISA kit (R&D Systems, Minneapolis, USA).

2.7.2. Arg-Gly-Asp (RGD) peptide patches immobilization

The RGD peptide immobilization protocol used in this project was adapted from (Yoon *et al*., 2003). The immobilization was carried out in two stages. First, the P(3HO)

material was aminated and films were cast. Then, the surface immobilization of the RGD peptide was carried out on one side of the aminated solvent cast films. Figure S1 shows the synthetic scheme for the RGD peptide immobilization in PHAs.

Preparation of aminated P(3HO):

In order to attach a terminal amine group to the P(3HO), the carboxylic acid terminal group was activated and reacted with hexaethyleneglycol-diamine. For this, 1 g of P(3HO) was dissolved in 10 ml of methylene chloride. 0.22 mmol of dicyclohexylcarbodiimide (DCC) and 0.22 mmol of N-hydroxysuccinimide (NHS) was added into the polymer solution with stirring. The reaction was stirred for 12 hr at the ambient temperature. Insoluble dicyclohexylurea was removed by filtration, and the carboxylic group activated polymer was isolated by precipitation in DMSO and dried for two days at the ambient temperature. The activated P(3HO) was reacted with an excess of hexaethyleneglycol-diamine (75 mg) in 10 ml of methylene chloride for 12 hr at the ambient temperature with stirring. The aminated P(3HO) was precipitated into cold ethanol.

Surface immobilization of RGD peptide on aminated P(3HO) films:

The film casting was carried out by dissolving 0.25 g of aminated P(3HO) with 0.25 g of non-aminated P(3HO) (50:50) in 10 ml of methylene chloride. After 5 minutes of vortexing, the solution was cast in a glass petridish and dried for 4 days at the ambient temperature. Dried films were pre-wetted in 70 % ethanol and washed in distilled water. Resulting films were hydrated in PBS for 4 hr. In order to introduce amine reactive groups onto the film surface, films were soaked in 20 ml of PBS containing 100 nM ethyleneglycol-bis-succinimidylsuccinate (EGS) and agitated for 4 hr at the ambient temperature. Films were washed with PBS three times and soaked in 20 ml of PBS

containing 30 nmoles of the RGD peptide. The solution was stirred for 12 hr at 4 ºC. The peptide immobilized films were washed with PBS and distilled water and then freeze-dried.

Confirmation of the RGD peptide immobilization on P(3HO) films:

The presence of the RGD peptide on the construct's surface was confirmed by FTIR, and contact angle analysis.

2.8. Cell adhesion and proliferation studies

2.8.1. Sample preparation

P(3HO) film patches were cut in to 1 cm^2 squares and sterilized under the UV light for 30 minutes each side. P(3HO) films were soaked in supplemented DMEM for 12 hr prior to cell seeding. Cell culture studies were performed in triplicates.

2.8.2. C2C12 cell seeding

C2C12 myoblast cells were grown in DMEM supplemented with 10 % of foetal calf serum, 1% w/v penicillin and 1 % w/v streptomycin solution and grown at 37 ºC with 5 % of CO_2. C2C12 myoblast cells in 70 % confluence were used for the cell seeding. Scaffdex® cell crowns were used to hold the cells on the well's surface. Around 20,000 cells were seeded on the pre-wetted patches in a 24 well plate. As a positive control, cells were seeded in the wells without films. For the negative control, films were incubated in supplemented DMEM without cells. Plates were incubated at 37 ºC with 5 % of CO2 and media was changed every 2 days. Cell proliferation was assessed at 24 hr.

2.8.3. C2C12 MTT assay

The (3-(4,5-Dimethylthiazol-2-yl)-2,5-diphenyltetrazolium bromide) MTT assay was performed on the patches containing the cells at 24 hr according to (Mosmann 1983). For this, 100 µl of a 5 mg/ml MTT solution in distilled water were added to each well at 24 hr and the plates were incubated for two hours at 37 ºC with 5% of CO2. After this, films were transferred to new 24 well tissue culture plates and 500 µl of DMSO was added. After a 5 minute incubation, 100 µl of the resulting solution were transferred to 96 well plates and the absorbance at 540 nm was measured on a Thermomax®microtitre plate reader. The absorbance of the samples were normalised with respect to the positive control. The difference in the surface areas of the tissue culture plate wells and the films were considered for the calculation of the % cell viability on the films.

2.8.4. C2C12 myoblast SEM

At 24 hr, patches containing the cells were visualized using SEM. To this end, cells were fixed in 0.1 M cacodylate buffer containing 3% glutaraldehyde for 12 hr at 4 ºC and dehydrated in a series of ethanol solutions (50 %, 70 %, 90 % and 100 %) for four times, incubating 10 minutes in each solution. Samples were air dried, coated and examined under the SEM.

2.9. Data analysis

Data are reported as mean ± STDEV. Statistical significance was assessed using ANOVA with the Newman-Keuls' test. Differences were considered statistically significant when $P<0.05$.

3. Results

3.1. P(3HO) patch production and structural characterization

The polymer was produced using *Pseudomonas mendocina* and purified as previously described (Rai *et al.,* 2011). Structural characterization of the resulting polymer was carried out by FTIR, GC-MS and NMR. The results obtained confirmed the presence of the P(3HO) homopolymer.

3.2. P(3HO) patch production and physical characterization

3.2.1. Mechanical properties

P(3HO) patches (5 wt%) were fabricated by solvent casting and mechanical characterization was carried out by dynamic mechanical analysis. The Young's modulus of the resulting patch was 3.7±0.3 MPa. The % elongation at break and the tensile strength, obtained at the maximum elongation, before the material is fractured was 299±3 % and 3.4±0.2 MPa, respectively. In a preliminary study, in order to understand the possible mechanical response of the patches to the body environment, mechanical properties were measured after incubating the samples in PBS buffer at 37°C for two hours. The Young's modulus, % elongation at break and the tensile strength were measured to be 1.5±0.4 MPa, 699.3±113 % and 10.1±1.4 MPa, respectively. Hence, at body temperature, the P(3HO) patch is less stiff, closer that of the myocardial stiffness of 0.02-0.5 MPa, has higher elongation at break and higher tensile strength, all features showing a further improvement over the measurements made at room temperature with a dry sample.

Controlled porosity in biomaterials is a key factor when they are used as a physical support for cell adhesion and growth (Lebourg *et al*., 2008). Porous P(3HO) patches were created by the particle leaching method and the effect of porosity on the mechanical properties was studied. For this, 0.5% sucrose with controlled particle size ranging from 250 to 300 µm was used as the porogen. Resulting patches showed a

percentage porosity of 28±5 %. Mechanical properties of the porous patches were measured. The obtained Young's modulus, tensile strength and elongation at break were 0.41±0.03 MPa, 0.7±0.1 MPa and 447±5 %, respectively. As described above, the Young's modulus of the human myocardium is 0.02-0.5 MPa, hence, the stiffness of the resulting P(3HO) porous patches was exactly in the range of the human myocardial structures, crucial to allow a synchronic beating of a myocardial engineered tissue.

3.2.2. *Thermal properties*

The thermal properties of the material were determined by differential scanning calorimetry analysis. The thermograms showed the presence of two peaks corresponding to the melting temperature and glass transition temperature. The melting temperature obtained was 43.7±4.1 ºC and the glass transition temperature was -32.9±3.8 ºC. The low melting temperature obtained together with a glass transition temperature below the ambient temperature indicates the elastomeric nature of the obtained P(3HO) polymer.

3.3. Functionalization of P(3HO) patches with fibres

3.3.1. P(3HO) fibre production

In order to mimic the fibrillar structure of the extracellular matrix which provides essential guidance for cell organization, survival and function, P(3HO) fibres were created by electrospinning. Electrospinning is a process based on the production of fibres by the application of a high voltage source to a polymer dissolved in a suitable solvent. For the optimization of the electrospinning conditions, a range of P(3HO) solutions were created in acetone (0.2 wt%, 0.5 wt%, 0.6 wt%, 0.7 wt%, 1 wt% and 1.2 wt%). The size of the fibres obtained in each condition was measured by optical microscopy and the results are shown in Table 1. It was observed that the fibre

diameters decreased with decreasing P(3HO) concentration and particles rather than fibres were obtained with the lowest concentration. In the case of 0.5 wt% P(3HO) solution, a transition between fibre formation and particle formation occurred, hence, both fibres and particles were obtained.

Table 1. Fibre and particle diameters obtained by electrospinning of different solutions of P(3HO) in acetone. Values are shown ± standard deviation.

P(3HO) concentration (wt%)	**Fibre diameter (nm)**	**Particle diameter (nm)**
1.2	750 ± 130	-
1	700 ± 100	-
0.7	630 ± 100	-
0.6	370 ± 90	-
0.5	340 ± 100	660 ± 60
0.2	-	580 ± 120

In order to determine the most suitable fibre or particle size to be used for the design of cardiac patches, fibres or particles were collected from the 1.2 wt%, 1 wt%, 0.7 wt%, 0.6 wt%, 0.5 wt% and 0.2 wt% polymer solution on glass slides for 10 minutes to ensure that the full surface of the slides were covered. In the following experiments cell proliferation on the P(3HO) fibres was assessed with the C2C12 myoblast cell line. Cells were seeded on the glass slides coated with different sizes of P(3HO) fibres or particles. Cell adhesion and proliferation were determined after 24 hrs using the MTT colorimetric assay. Figure 1 shows the results obtained. Our

results showed that an increment in fibre diameter resulted in a higher % cell proliferation, achieving the highest value of 196.8± 16.0 with 750 nm fibres. Also, cells showed preference for fibrous structures as compared to particle structures.

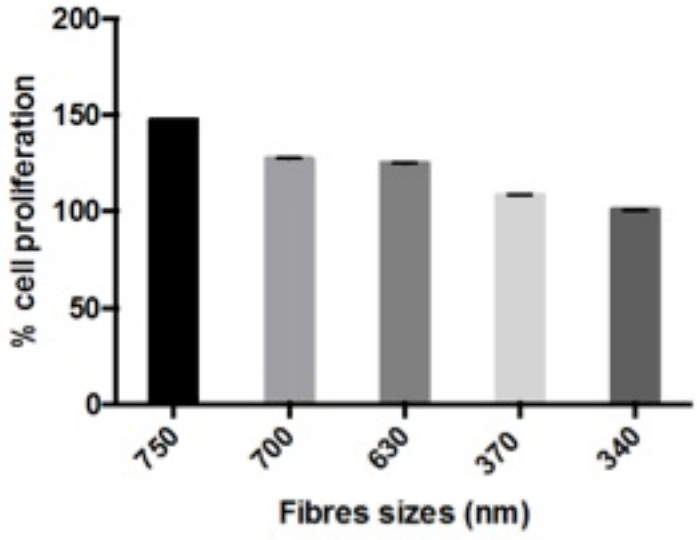

Figure 1. The percentage cell proliferation of C2C12 cell line normalized against cell growth on tissue culture plastic (n=4; error bars=±SD). Mean ± sem, n=4. An increment in fibre diameter resulted in a significant increment in % cell proliferation, One-way ANOVA $P<0.05$.

Several studies have shown that fibrous matrices, which allow cell infiltration into their porous structure, are attractive substrates as tissue engineering scaffolds (Lee *et al*., 2011, Krupnick *et al*., 2001). Pores in an electrospun fibrous structure are formed by nonaligned fibres and the size and shape of those pores will be directly related to the fibre concentration. In order to find the optimal concentration of fibres that will allow cell infiltration, in the next experiment, the collection times for the 750 nm fibres on glass slides were varied from 1 to 90 seconds and the fibre concentration was evaluated by optical microscopy. The selected collection time was 30 seconds, in which the fibres covered the entire surface, leaving some gaps for the cells to infiltrate.

3.4. P(3HO) surface characterization studies

The surface structure of the neat P(3HO) and porous patches with or without fibrous structures was characterized in terms of wettability, roughness and SEM. The surface wettability of the patches was studied with a contact angle meter. The water contact angle on the neat P(3HO) patches was 101.1±0.8º, indicating a hydrophobic surface. The obtained water contact angle for the porous patches was 104.9 ± 6.0º. The water contact angles measured for the plain and porous patches functionalized with fibres were 110.2± 3.7 for neat P(3HO) patches containing 750 nm fibres and 99.8 ± 1.9 for porous patches containing 750 nm fibres. Surprisingly, an increment in the surface hydrophobicity was observed when neat patches were functionalized with fibres and a decrease in the surface hydrophobicity was observed when porous patches were functionalized with fibres.

The surface roughness properties of the different patches was studied. Results indicate that the average surface roughness of the P(3HO) neat and porous patches was 0.17 µm and 0.9±0.2 µm, respectively. The average surface roughness of the patches functionalized with fibres was 0.90±0.01 µm for neat patches and 1.1±0.1 µm for porous patches. As expected, an increment in the surface roughness was observed when patches were functionalized with fibrous structures, achieving the maximum roughness when porous and fibrous structures were combined.

Finally, the surface morphology and microstructure of the P(3HO) neat and porous patches was visualized using scanning electron microscopy.

3.4.1. In vitro cell proliferation studies

As the structure of the P(3HO) fibres was intended for cardiac tissue engineering, its suitability was initially evaluated *in vitro* using C2C12, a myoblast cell line. Cells were seeded on the cardiac patches and the % cell proliferation was assessed at 24 hrs with the MTT colorimetric assay. Cell proliferation results for the different patches were compared. The results showed that the % cell proliferation increased 2.5 fold when porous structures were incorporated on the P(3HO) patches (Figure 2). Additionally, a significant increment in the % cell proliferation was obtained when fibre structures were incorporated on the surface of the neat P(3HO) and porous patches. Similar values for cell proliferation were observed with the porous and neat patches modified with fibres, suggesting that both structures contribute in a similar way to cell proliferation. Finally, P(3HO) porous patches containing the P(3HO) fibrous structures showed the highest cell proliferation rate and hence this was the best matrix for cell adhesion and proliferation.

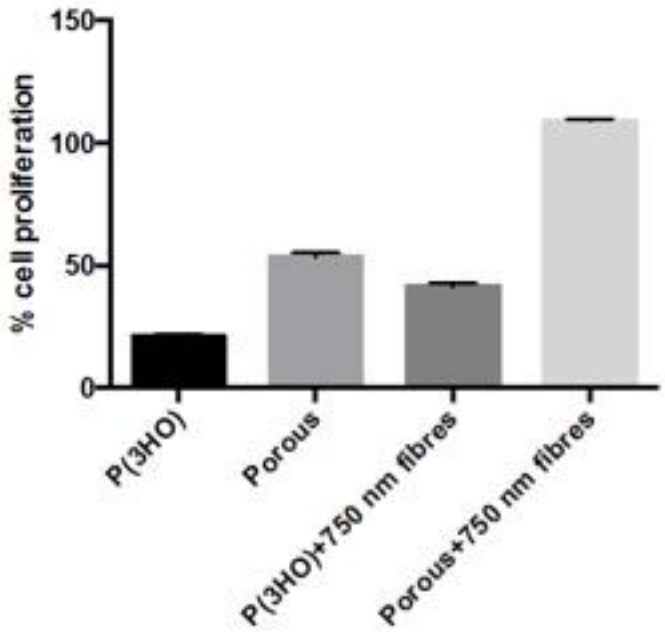

Figure 2. The % cell proliferation of C2C12 cell line on neat P(3HO) patches containing porous structures, fibrous structures and both fibrous and porous structures.

Results were normalized against cell growth results on tissue culture plastic, used as a control. Mean ± sem, n=4. % cell proliferation was significantly greater when porous or fibres were incorporated on to the P(3HO) patches, One-way ANOVA $P<0.01$.

SEM analysis was carried out to visualize the C2C12 myoblast cell line on the neat and porous P(3HO) patches with and without fibres. Figure 3 shows typical SEM images observed for samples after 24 hr of cell growth. These results showed that at 24 hr the surface of the porous cardiac patches is covered with cells and that cells grew inside the pores, almost covering the pore structures. For P(3HO) patches functionalized with fibrous structures, it is possible to observe cells growing on top of the first cell layer.

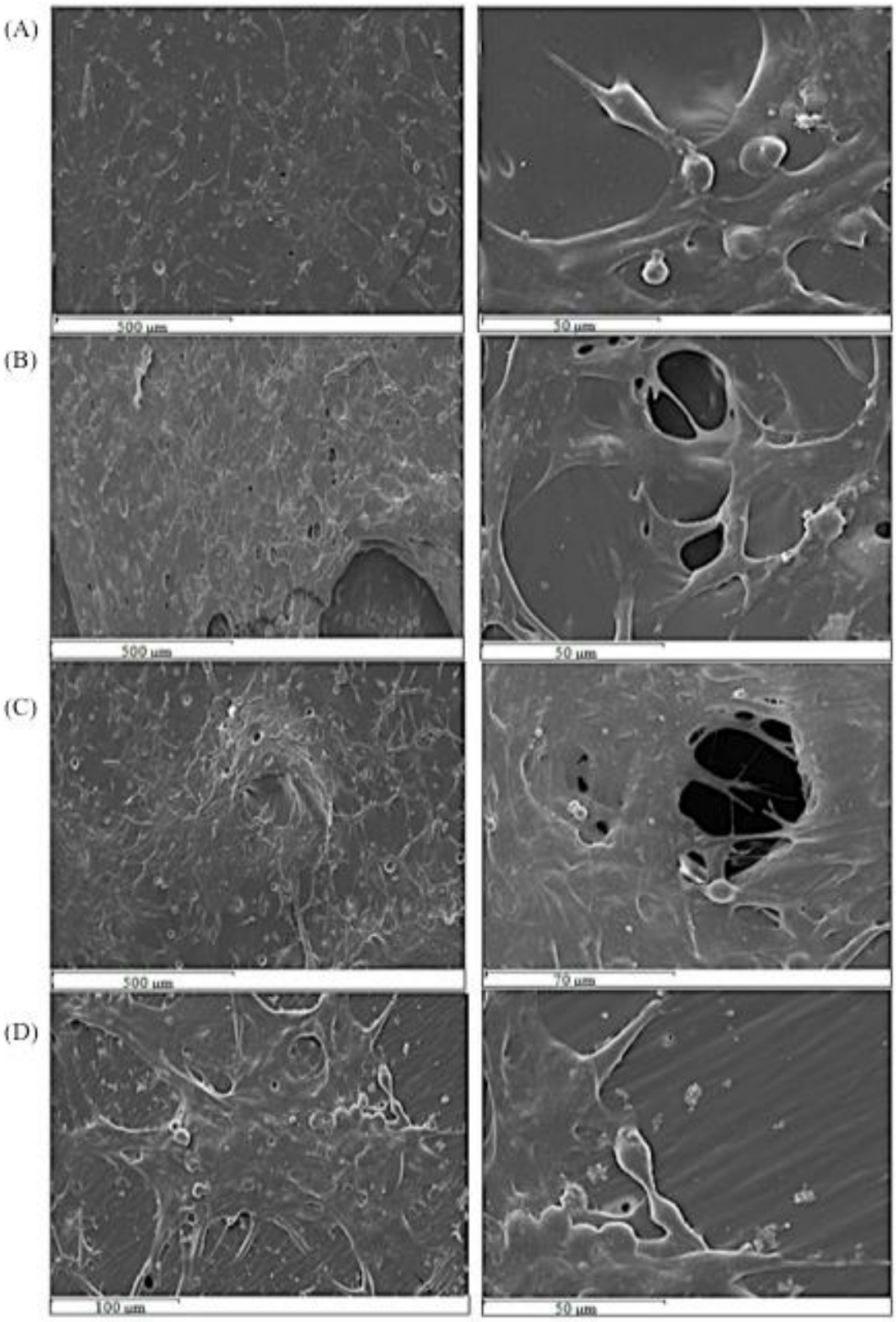

Figure 3. SEM images of C2C12 cells at 24 hr on P(3HO) A) neat polymer patches, B) porous patches C) neat polymer patches modified with 750 nm fibres and D) porous patches modified with 750 nm fibres.

3.5. Cardiomyocyte cytocompatibility studies

3.5.1. Cardiomyocyte viability on P(3HO) patches

The biocompatibility of the P(3HO) polymer was further assessed by comparing the number of live/dead NVRM cells on both P(3HO) patches and collagen coated wells. The ratios of live/dead NVRM cells are illustrated in Figure 4. These results show similar viability on both P(3HO) polymer and collagen, showing that P(3HO) is equally biocompatible towards cardiomyocytes as compared to collagen, the current gold standard for cardiac tissue engineering. Figure 5 shows confocal microscopy images of the NVRM cells labeled with ethidium homodimer-1 growing on P(3HO) polymer and collagen, and anti α-actinin and DAPI immunofluresent imaging, showing NVRM cells growing on P(3HO patches and forming well-formed sarcomeres, confirming high biocompatibility of the patches.

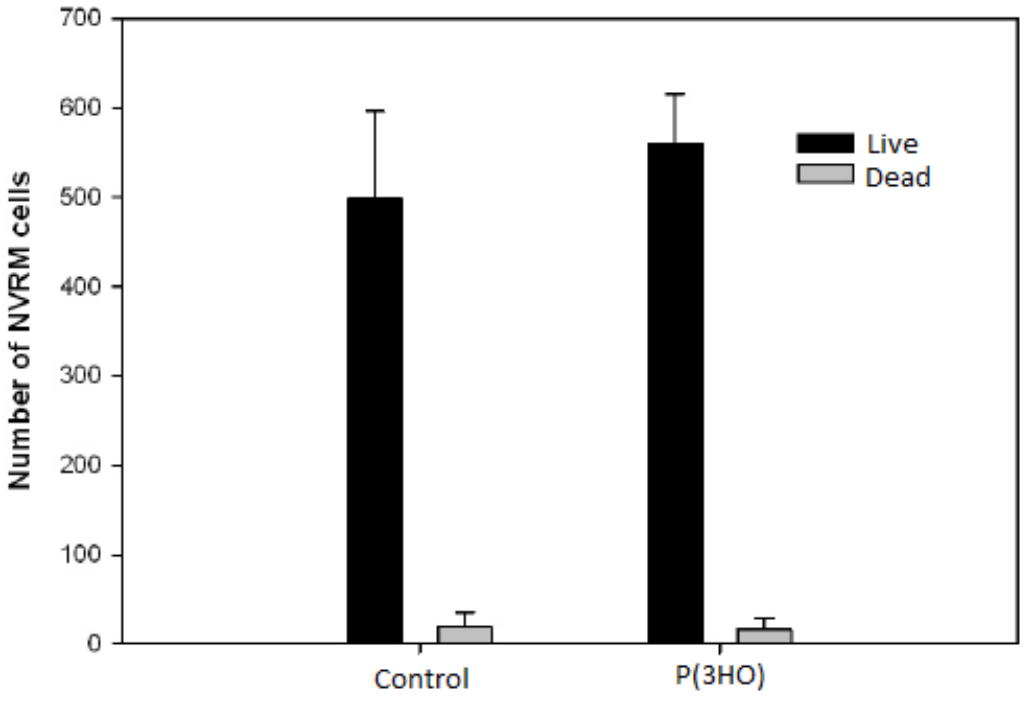

Figure 4. Number of live/dead NVRM cells two days after plating on P(3HO) patches

and collagen. Mean ± sem, n=3 experiments. No significant differences were observed between the number of live/dead cells on P(3HO) and collagen.

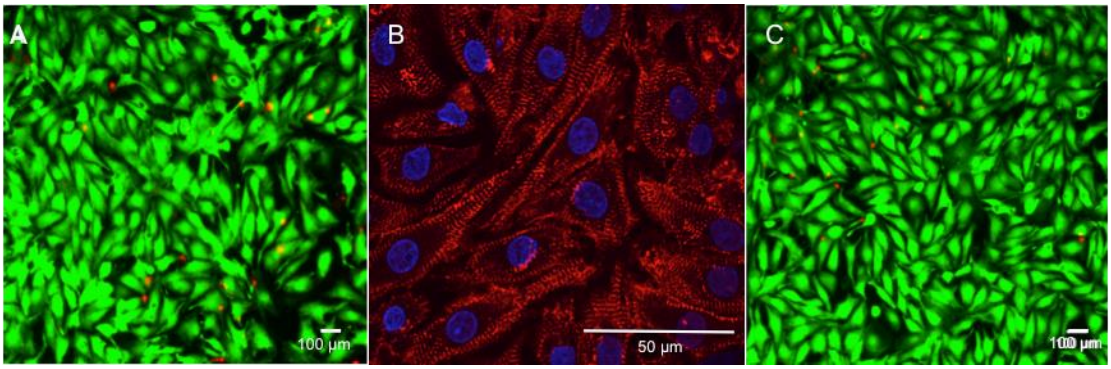

Figure 5. Confocal microscopy images of NVRM cells labeled with ethidium homodimer-1 grown on (A) control collagen and (B) P(3HO) patches. Green indicates live cells while red depicts the dead cells.

3.5.2. Cardiomyocytes' contraction on P(3HO) patches

The effect of the P(3HO) polymer on the contraction of the cardiomyocytes was studied. Fresh isolated adult rat cardiomyocytes were seeded on P(3HO) coated cover slips and superfused in a Krebs-Henseleit solution at 37°C and bubbled with 95% O_2, 5% CO_2. Cover slips without coating were used as controls. For the study, rod shaped cardiomyocytes with regular stimulated contractions but no spontaneous contraction without stimulation were selected. Cells were stimulated with pulses of 50 V for a period of 2ms with 2 second intervals. The contraction amplitude (% shortening), time to peak 90% and time to relaxation 50% were recorded with a video and analyzed with the Inoptix program.

The effect on cardiomyocyte contraction with P(3HO) polymer as the substrate, when cells were stimulated at a range of electrical pulses and calcium concentrations, was studied. Figure 6A shows the effect on cardiomyocyte contraction (% shortening) for

both polymer and control when the intervals of electrical pulses were varied for 2, 5, 2, 1 and 0.5 second interval. No differences were observed in % shortening between polymer and control. A significant reduction in % shortening was observed in the control when the intervals of electrical pulses decreased from 5 to 2, 1 and 0.5 seconds but not in the polymer. These results indicate the capacity of the cardiomyocytes to maintain a sustained contraction capacity when P(3HO) was used as the substrate, an essential and excellent property for Cardiac Tissue Engineering.

The calcium concentration in the Krebs-Henseleit solution was increased from 1 to 2, 3 and 4 mM when P(3HO) or glass coverslips were used as the base matrix. Figure 6(B) shows the effect on cardiomyocyte contraction (% shortening) at 1, 2, 3 and 4 mM calcium for both polymer and control. There was a tendency for contraction to increase with increasing calcium, but no significant difference was observed between the control and P(3HO) at any concentration.

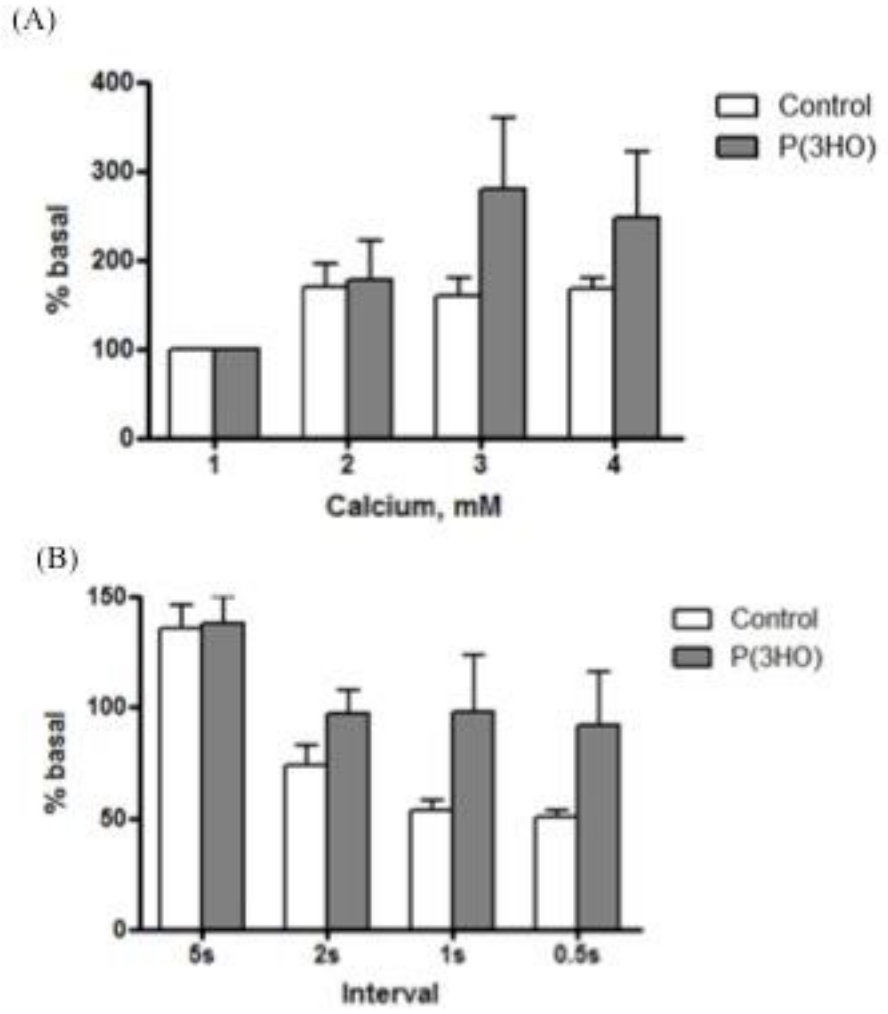

Figure 6. (A) Normalised contraction amplitude (% shortening) of adult rat cardiomyocytes at different beating frequencies on P(3HO) polymer or glass cover-slips. Mean ± sem, n=5 cells from separate preparations. 2 way ANOVA shows a significant effect of frequency $P<0.001$ but no difference between P(3HO) and control. **(B)** Normalised contraction amplitude (% shortening) of adult rat cardiomyocytes with increasing extracellular calcium on P(3HO) polymer or glass cover-slips. Mean ± sem, n=5 cells (control) and 3-4 cells (polymer) from separate preparations. No significant differences between P(3HO) and control.

Table 2(A) and 2(B) show 'time to peak 90%' and time to 'relaxation 50%' for control and P(3HO) polymer at different interval of pulses and different calcium concentrations, respectively. Contraction amplitude (% shortening) decreased significantly with reduced interval, but there was no significant difference between behaviour on polymer vs. control. Results showed no differences in 'time to peak 90%' and time to 'relaxation 50%' between polymer and control.

Table 2. 'time to peak 90%' and time to 'relaxation 50%' when cardiomyocytes were stimulated at a range of electrical pulses of 50 V for 2 ms at 2, 5, 2, 1 and 0.5 second interval. Results are shown ± SD. **(B)** 'time to peak 90%' and time to 'relaxation 50%' when cardiomyocytes were stimulated at a range of electrical pulses of 50 V for 2 ms at 2 second interval when calcium concentration was increased from 1 to 2, 3 and 4 mM. Results are shown ± SD.

(A)

	Time to peak 90% (sec)		Time to baseline 50% (sec)	
Intervals (sec)	Control ± SD	Polymer ± SD	Control ± SD	Polymer ± SD
2	0.058±0.011	0.051±0.010	0.118±0.011	0.105±0.011
5	0.060±0.017	0.056±0.013	0.132±0.019	0.114±0.013
2	0.056±0.018	0.053±0.013	0.109±0.018	0.113±0.015
1	0.049±0.007	0.053±0.011	0.098±0.008	0.109±0.012
0.5	0.047±0.008	0.050±0.009	0.095±0.022	0.107±0.033

(B)

	Time to peak 90% (sec)		Time to baseline 50% (sec)	
Calcium (mM)	Control ± SD	Polymer ± SD	Control ± SD	Polymer ± SD
2	0.052±0.009	0.055±0.010	0.101±0.010	0.113±0.010
3	0.059±0.008	0.053±0.007	0.112±0.009	0.115±0.008
4	0.058±0.010	0.049±0.010	0.111±0.011	0.132±0.018

3.6. P(3HO) functionalization with active molecules

3.6.1. RGD immobilization

The cell-polymer and cell-cell interactions play a key role in controlling cell adhesion, proliferation, migration and differentiation. Several reports show the role of the RGD peptide in controlling these interactions (Yoon *et al*., 2003, Hersel *et al*., 2003, Rezania and Healy 2008). In order to improve the properties of the P(3HO) cardiac patches, RGD peptides were immobilized onto the surface of the patch. The RGD peptide immobilization protocol used in this work was adapted from (Yoon *et al*., 2003), where RGD motifs were immobilized on PLGA. Firstly, the carboxylic acid terminal group of P(3HO) was aminated by reacting the polymer with hexaethyleneglycol-diamine. FTIR was carried out to confirm that the amination had occurred. The FTIR spectrum obtained from the modified P(3HO) patch was compared with the neat P(3HO) polymer patch. Results show the presence of a band at 3400 cm-1, which corresponds to the N-H bond. Additionally, a band was observed at 1000 cm^{-1} confirming the presence of a C-N bond. These absorbance peaks were missing in the neat polymer patch. This result confirmed that the P(3HO) patch had been successfully aminated. The aminated P(3HO) polymer was blended with equal amounts of P(3HO) (50:50) and patches were

fabricated by the solvent casting technique. The resultant patches were modified with RGD tripeptides on one side of the structure. In order to verify the presence of RGD motifs covalently linked to the membrane, FTIR was carried out. The FTIR spectra obtained from the RGD immobilized P(3HO) film was compared with the as synthesized P(3HO) film. Results showed the presence of a strong band at 1287 cm-^{1} corresponding to the C-N bonds present on the RGD-P(3HO) polymer. Also, other bands were observed at 825 cm^{-1}, 1047 cm-^{1} and 1226 cm^{-1} due to the bend of the N-H bond and the stretch of C-O and C-O-C bonds from the poly(ethylene glycol) (PEG) group linked to the structure, respectively. Finally, as expected, the band observed at 3400 cm-^{1} corresponding to the $–NH_2$ functional group was not observed in this case. This is due to the fact that this terminal amine group would have reacted with the RGD sequence and hence the new terminal group is the carboxylic group from the RGD peptide.

Previously various groups have shown the relation between RGD immobilization and surface wettability. It was observed that the incorporation of RGD structures on the surface of the polymer has a direct effect in decreasing the hydrophobicity of the structure. In order to confirm the presence of RGD motifs linked to the P(3HO) cardiac patches, the surface wettability of the cardiac patches was analysed. The water contact angle obtained for the P(3HO)-RGD film was 93.4±0.1°. P(3HO) water contact angle was 101.1±0.8º . Our results show a significant decrease in the water contact angle, which indirectly confirms the presence of the RGD immobilized peptide.

As described previously, mechanical properties of the cardiac patch play an essential role in the patch function supporting the heart during regeneration. In order to study the possible influence of the P(3HO) modification on the patch mechanical properties, dynamic mechanical analysis was carried out on P(3HO)-RGD cardiac patches. The

Young's modulus of the RGD modified film was 3.9 MPa. The P(3HO) neat patches' Young's modulus was 3.7±0.3 MPa, hence no differences were observed in terms of the material stiffness after the RGD modification. The tensile strength for P(3HO)-RGD was 0.7 MPa and elongation at break 426.5%. The tensile strength and elongation at break for P(3HO) was 3.4±0.2MPa and 299±3 %, respectively. These results show a decrease by 19% in tensile strength and an increase by 42% in elongation at break after the RGD modification. In order to visualize the surface of the modified cardiac patches, SEM was carried out. Figure S2 shows the SEM images of P(3HO)-RGD cardiac patches. These pictures revealed that the incorporation of RGD peptide structures changed the surface morphology of the patch by introducing a rough topography on the surface.

3.6.2 VEGF incorporation in P(3HO) patches

As vascularisation and angiogenesis are key factors in cardiac tissue engineering, VEGF was incorporated into the P(3HO) patches. The mechanical properties of the resulting cardiac patches were measured. The Young's modulus obtained for the VEGF modified film was 6.8 MPa, the tensile strength was 0.6 MPa and the elongation at break was 449.3%. The tensile strength and elongation at break for P(3HO) was 3.4±0.2 MPa and 299±3 %, respectively. These results show a decrease in tensile strength by 17% and an increase by 50% in elongation at break after the VEGF incorporation. The surface of the VEGF modified cardiac patches was analysed by water contact angle measurement and SEM. The water contact angle of the P(3HO) cardiac patches containing VEGF factor incorporated was 102.5 ± 1.4° and that of neat P(3HO) was 101.1±0.8 °. These results show no differences in the surface wettability with VEGF incorporation.

3.6.3. Cell proliferation on RGD and VEGF patches

The effect of P(3HO)-RGD immobilized cardiac patches and P(3HO)-VEGF on cell proliferation as compared to the neat polymer patch was studied. C2C12 myoblast cells were seeded on P(3HO) modified cardiac patches and cell proliferation was measured by the MTT colorimetric assay. Figure 7 shows the % cell proliferation on P(3HO), P(3HO)-VEGF, P(3HO)-RGD and P(3HO)-VEGF+RGD cardiac patches when proliferation observed on tissue culture plastic was considered to be 100%. The % cell proliferation on P(3HO) patches was 21.11±5.29 %. A significant increase in cell proliferation was observed when VEGF and RGD were incorporated into the P(3HO) cardiac patches. However, a higher cell proliferation was achieved with VEGF. A synergistic effect was observed when both VEGF and RGD were incorporated together, showing a highly significant effect on cell proliferation.

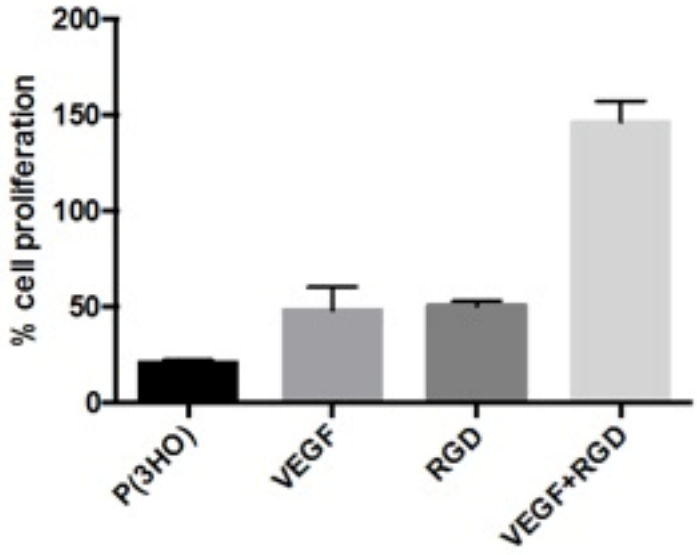

Figure 7. The % cell proliferation of C2C12 cell line at 24 hr on P(3HO), VEGF, RGD and VEGF+RGD modified P(3HO) patches. Mean ± sem, n=4. % cell proliferation significantly greater when VEGF or RGD were incorporated to the P(3HO) patches, One –Way ANOVA.

3.6.4. VEGF release

The cumulative *in vitro* release of VEGF from P(3HO) cardiac patches was studied over 30 days. The amount of VEGF released in the medium was measured using the Invitrogen® VEGF human ELISA kit. The release profile is shown in Figure S3. Our results showed a biphasic VEGF release for P(3HO) cardiac patches with an initial burst release followed by a period of sustained release.

4. Discussion

Medium chain length PHAs, with a typical monomer chain length from 6-16 carbon atoms, are polymers produced by bacteria. Mcl-PHAs are of great interest because according to the number of carbons in the side chain, the physical properties of these biodegradable polymers can be varied, allowing the production of tailor made functional materials. Previous reports have shown that mcl-PHAs are flexible elastomeric polymers, with low crystallinity, low glass transition temperature, low tensile strength, and high elongation to break (Zinn *et al*., 2001). In this work we studied poly(3-hydroxyoctanoate), a mcl-PHA, as a potential novel functional material for cardiac tissue engineering. P(3HO) was known to be produced as a homopolymer by *P. mendocina*, as previously described (Rai *et al*., 2011).

4.1. P(3HO) engineered patches

Engineering biomaterials to promote cell adhesion and direct cellular behavior is crucial for the development of materials capable of restoring tissue function. Several reports have proven that cells are sensitive to the physical and chemical environment which determines cell specific migration, proliferation, differentiation and production

of proteins which in turn influences tissue organization and regeneration (Shin *et al*., 2004). Several studies on creating beating engineered synthetic patches have been reported recently showing that the stiffness of the scaffold impeded the contractions (Shin *et al*., 2004). Additionally, due to the myocardial tissue cyclic and constant beating, a plastic deformation and failure is expected when thermoplastic polymers such as polyglycolic acid (PGA), polylactic acid (PLA) and poly(ε-caprolactone) (PCL) and their copolymers are exposed to long term cyclic strain. Table 3 shows the mechanical properties of some of the materials that have been explored for myocardial tissue engineering. These data show that most natural materials are weaker than myocardial structures in contrast to synthetic materials, which are much stiffer than the human myocardium.

Table 3. Mechanical properties of materials proposed for myocardial tissue engineering

Polymer	Young's modulus	Tensile strength	References
Collagen	2-22 KPa	1-9 KPa	Roeder *et al.*, 2002
Alginate	10-50 KPa	10-40 KPa	Drury *et al.*, 2004
PGA	7-10 GPa	70 MPa	Webb *et al.*, 2004
PCL	343.9-364.3 MPa	10.5-16.1MPa	Eshraghi and Das 2010
PLA	1-4 GPa	30-80 MPa	Garlotta 2001
PLGA	67 MPa	4 MPa	Lin *et al.*, 2011
Myocardium (human)	0.02-0.5 MPa	3-15 KPa	Watanabe *et al.*, 2006 Nague *et al.*, 2004

Although most synthetic materials do not have the desirable mechanical properties for cardiac tissue engineering applications, some of these polymers can be tuned by

introducing different structures in the polymer backbone. Among the different synthetic polymers, polyurethanes seem to be the most versatile due to their large number of building blocks (macrodiols, diisocyanates and chain extenders) that allow the introduction of peptide sequences and several types of biomolecules in the polymeric chain (Silvestri *et al.,* 2014). However, different polyurethanes have shown various problems such as hydrolysis, oxidation, environmental stress cracking, thrombosis and calcification *in vivo* (Guan *et al*., 2005, Ma *et al*., 2012, Santerre *et al*., 2005). Hence, several groups have worked towards improving the polyurethane properties via incorporation of peptide sequences and biomolecules to the polyurethanes chain to achieve the desirable properties active tissue engineering. Guan *et al.,* 2008 and Silverstri, *et al.,* 2013 have focused on the enhancement of the polyurethane elasticity, strength and biodegradable properties. A biodegradable polyurethane containing an elastase-sensitive peptide sequence was developed. Although the mechanical, biological and biodegradation properties were improved *in vitro*, *in vivo* experiments need to be carried out to test the capability of the patches to recruit cardiac cells and restore mechanical and biological functions of the infarcted ventricle.

In this work we have looked in to the development of cardiac patches using a relatively unexplored family of polymers, polyhydroxyalkanoates, more specifically, P(3HO). In the first part of this work, P(3HO) based plain and porous patches were created by the solvent casting and solvent casting particle leaching, respectively. Porosity was incorporated in order to allow cell ingrowth. As P(3HO) is a biodegradable material, it is anticipated that the biomaterial structure will reabsorb leaving behind new tissue. The average diameter of the pores was 250-300 μm, which is close to the size of adult human myocytes. It is important to mention that although porous structures provide more surface for cell residence, the number of porous structures that can be created are

limited by the desired mechanical properties of the biomaterial. Materials with high porosities displayed diminished mechanical properties (Golstein *et al*., 1995). As one of the main requirements for a biomaterial in cardiac tissue engineering is to support the high mechanical demands of the organ during regeneration, the porogen concentration, which would determine the porosity in the patch, was chosen to allow some cell ingrowth without substantial deterioration of the mechanical properties. For this, P(3HO) porous patches were made using 0.5 wt% polymer solution. The resulting patches were fully characterized and assessed for cardiac tissue engineering applications. The mechanical properties of the material plays a crucial role in supporting the injured organ during regeneration. The P(3HO) patches' mechanical properties were measured before and after the samples were incubated in PBS at 37°C. As myocardial stiffness is considered to be an essential myocardial property, especially during the diastole, stiffness was quantified by examining the relationship between stress and strain (Nagueh *et al*., 2004). The Young's modulus of the P(3HO) neat film before and after incubation in PBS at 37°C was 3.7±0.3 MPa and 1.4±0.4 MPa, respectively. Hence, although a decrease in the P(3HO)'s stiffness was observed after incubating the samples in PBS buffer at 37°C, the obtained value was in fact closer to the Young's modulus value of the human myocardium (0.02-0.5 MPa), an excellent improvement. In addition, the Young's modulus value of the porous film was 0.41±0.03 MPa, which is exactly within the range of the stiffness of the human myocardium. As the lower value of myocardial stiffness is 0.02 MPa, it is possible to further increase the number of porous structures and decrease the stiffness of the construct even further. However, as after a myocardial infarction there is an increasing load on the heart wall we hypothesized that among the range of cardiac patches, the one with a higher stiffness is best suited for myocardial support (Sutton and Shape 2000). The ability to resist

failure under tensile stress is one of the most important properties of materials used in structural applications. The tensile strength obtained for P(3HO) patches before and after incubation in PBS at 37°C and porous patches were 3.4±0.2 MPa, 10.1±0.4 MPa and 0.7±0.2 MPa, respectively. Although these values are higher than myocardial structures (human myocardium tensile strength 3-15 kPa), a higher tensile strength might have a positive effect as after a myocardial infarction, the abrupt loss of myocardium triggers a ventricular remodeling that includes dilatation, hypertrophy, and the formation of a collagen scar that increases the load on the infarcted region. Furthermore, it has been described that negative ventricular remodeling continues for weeks or months until the distending forces on the cardiac tissue are counterbalanced by the tensile strength of the collagen scar, hence, a higher tensile strength could have a positive effect after a myocardial infarction (Sutton and Sharpe 2000) Finally, the percentage elongation at break of neat P(3HO) patches before and after incubation in PBS at 37ºC and porous patches was 299±3 %, 699±113 % and 447±5 %, respectively. These values show that neat P(3HO) polymer patches have an elongation at break in the range of myocardial structures and this value is somewhat higher for both the neat P(3HO) patch incubated in PBS at 37°C and porous patches (human myocardial elongation at break is between 100-300 %). This further confirms the suitability of P(3HO) based cardiac patches for myocardial repair and regeneration.

In order to define the processability of the material, the thermal properties of the polymer were determined by differential scanning calorimetric analysis. Thermal analyses of P(3HO) showed two peaks corresponding to the glass transition temperature and melting temperature observed at -32.9±3.8 ºC and 43.7±4.1 ºC during the first heat scan, respectively. A glass transition temperature below ambient temperature and the low melting temperature, which reflects the low crystallinity of the polymer imparts an

elastomeric behavior to the material. Although the melting temperature of P(3HO) is quite close to the human body temperature, the mechanical testing carried out in PBS, at 37ºC, described above, have proven that the mechanical properties of the P(3HO) patches remain suitable for cardiac tissue engineering, i.e., the Young's modulus, tensile strength and elongation at break values remain similar to that of the myocardium.

4.2. Surface functionalization

The extracellular matrix provides not only structural support to the cells but also regulatory cues for cells assembling into tissues, for growth and communication. As a result, one of the main goals in tissue engineering is to develop a tailored *in vitro* environment that mimics the intricate and organized mesh of native extracellular matrix. As the extracellular matrix is mainly composed of collagen fibrils, the structure and topography of the fibres were recreated by electrospinning. Electrospinning is a versatile technique which allows the fabrication of nano and micro scale fibres or particles which mimic the extracellular matrix architecture. Different P(3HO) concentrations ranging from 0.2 wt% to 1.2 wt% were used to create electrospun fibres. The results obtained showed an increment in the fibre diameter from 340 nm to 750 nm when the polymer concentration was increased from 0.6 wt% to 1.2 wt% (Table 1). These results were in agreement with Boland *et al.*, (2001) who showed a direct relation between polymer concentration and electrospun fibre diameter (Boland *et al.*, 2001). When the P(3HO) concentration was 0.5 wt%, both fibres and particles were obtained. Only particles were obtained with 0.2 wt% polymer solution.

In order to find out the most suitable matrix for cells to grow, glass slides were coated with the different fibre sizes obtained. C2C12 myoblast cells were seeded on the

electrospun coated slides. The results obtained showed that the fibre diameter has a direct effect on cell adhesion and proliferation, with an increment in cell density with fibre size. The adhesion of cells to the extracellular matrix is mediated through focal adhesions, large protein complexes organized at the basal surface of cells, which connects the cytoskeleton of the cell to the matrix. Previous studies have shown that differences in fibre diameter result in highly significant differences in focal adhesion formation and cell proliferation (Hsia *et al*., 2011). In contrast to our results, Chen *et al*., (2007) observed an increment in fibroblast adhesion as a function of decreasing electrospun polycaprolactone fibre diameter from 1051 to 428 nm (Chen *el al.*, 2007). We hypothesize that differences observed in these studies may be related to differences in cell size, however, further studies should be carried out to elucidate how the fibre size affects cell adhesion and proliferation.

It is important to mention that fibre diameter also has a crucial role in controlling the pore diameter of the networks. It has been proven that increasing fibre diameter results in an increase in mean pore radius and hence cellular ingrowth. (Eichhorm and Sampson 2005). Previous findings have shown that nanofibre structures impede cell migration into the scaffolds as they act as a sieve, keeping cells on the surface of the scaffold (Balguid *et al*., 2009). In order to allow cell migration into the interior of the electrospun fibres and porous structures, different collection times were assessed. The selected collection time was 30 seconds, the one in which the fibres have covered the full area leaving gaps for the cells to infiltrate. Although some pores were smaller than myocardial cells, they should not impede cell migration as the fibres are lying loosely upon each other and cells perform amoeboid movements to migrate through the pores by pushing fibres (Laurencin *et al*., 2002).

4.3. Surface characterization

The surface of the biomaterials plays a significant role in determining the outcome of the biological system and biomaterial interaction (Flemming *et al*., 1999). The hydrophobicity of a biomaterial surface is directly related to cell adhesion. The cell adhesion to a surface occurs by adhesion receptors present in the cell that binds to proteins adsorbed on the surface and the conformation of these proteins depends on the surface wettability (Lee *et al*., 2003). It has been described that the water contact angle of hydrophobic surfaces is higher or equal to 90º (Li 2011). The P(3HO) patches' water contact angle was 101.1 ± 0.8º for neat polymer patches and 104.9 ± 6.0 º for porous patches. For the patches modified with fibres the water contact angle measured was 110.2± 3.7 for neat P(3HO) patches containing 750 nm fibres and 99.8 ± 1.9 for porous patches containing 750 nm fibres. An increment in the surface hydrophobicity was observed when neat patches were functionalized with fibres and a decrease in the surface hydrophobicity was observed when porous patches were functionalized with fibres. It has been described that the wettability depends on the type of material as well as the surface treatment of the material (Lu and Chung 1998). Our results show that the P(3HO) patches' surface is hydrophobic, however, the value is not much higher than the upper limit of 90º, known for hydrophilic surfaces. In general, hydrophilic surfaces display better affinity for cells as compared to hydrophobic surfaces (Lampin *et al*., 1997), however, our biocompatibility test results confirmed the excellent cell attachment and proliferation on the P(3HO) patches, comparable to that of collagen. This indicates the possible adherence of media proteins on the surface of the P(3HO) which in turn results in excellent cell attachment and proliferation properties.

With regard to roughness of the surface affecting the growth of different kinds of cells, most researchers have shown that increased surface roughness has a positive effect on

cell adhesion (Richert *et al*., 2008). The surface roughness of the film was measured using the white light interferometry technique. The surface roughness of the cardiac patches was 0.90±0.01 µm for neat patches with 750 nm fibres and 1.1±0.1 µm for porous patches with 750 nm fibres. The surface roughness of the neat and porous P(3HO) patches was 0.2 µm and 0.9±0.2 µm. These results showed that the incorporation of porous and fibrous structures increases the surface roughness by approximately 5 fold and by 6.5 fold, respectively, a positive feature for a material to be used for the development of a cardiac patch.

SEM analysis and surface roughness studies revealed that the P(3HO) neat polymer patches present a smooth surface. The visualization of the fibres by SEM was not possible due to the high temperature sensitivity of the P(3HO) fibrous structures which melted under the SEM focused beam of high-energy electrons.

Several groups show the influence of surface wettability and roughness in the cell-biomaterial interaction, however, no general principles that can help in the prediction of cellular behavior by the combination of these parameters are known. Therefore, cell adhesion and proliferation were assessed. Myoblast (C2Cl2) cell proliferation was analyzed and compared on neat P(3HO) patches, porous patches, neat P(3HO) polymer cardiac patches with 750 nm diameter fibres and porous cardiac patches with 750 nm diameter fibres on their surface. The proliferation observed on these patches were 21.1±1.9 %, 53.8±3.1 %, 41.6±2.4 % and 109.2±1.5 %, respectively, when proliferation observed in tissue culture plates was considered to be 100 %. Results showed that both porous and fibrous structures increased the % cell proliferation due to their higher surface area-to-volume ratio as well as their topographical features that can enhance cellular adhesion and proliferation. A higher cell proliferation was observed when porous structures were incorporated than with fibrous structures. P(3HO) porous

patches modified with 750 nm fibres resulted in the best matrix for C2C12 cells to proliferate .

Thus results from this study suggests that the P(3HO) porous cardiac patches functionalized with 750 nm fibres are promising materials to support the infarcted myocardium, due to their mechanical properties and ability to deliver cells in order to allow efficient tissue regeneration caused by their good cell adhesion properties.

4.4. Use of P(3HO) as a novel functional material in cardiac tissue engineering

The heart wall is composed of a high density of cardiomyocytes and fibroblasts with abundant vascular network and collagen based extracellular matrix (ECM). Native tissue matrix serves as a structural and informational template for cell attachment and tissue formation (Gupta *et al.,* 2006). In this work, the P(3HO) patches were proposed as an alternative for the extra cellular matrix (ECM), therefore, their cell adhesiveness and proliferation will directly affect number of adhered cells and hence the quality of the engineered tissue. In this study NVRM cells were grown on both P(3HO) and collagen and the cell attachment, viability and proliferation was compared. Our results have shown that P(3HO) was as good as collagen in terms of cell attachment, viability and proliferation, however, with respect to mechanical integrity, degradation rate, processability and the fact that it is a non-animal source polymer are distinctive advantages of the P(3HO) patches as compared to that of collagen.

The proper contraction of individual cardiomyocytes is essential for the normal functioning of the heart. Intracellular calcium is the main factor that regulates cardiomyocyte contraction. First, an action potential leads to the opening of L-Type calcium channel present in the membrane of the cells. Second, the calcium entering the cells triggers the release of calcium from the sarcoplasmatic reticulum, leading to a

marked increase of cytosolic calcium concentration. High concentrations of intracellular calcium initiate the interaction of contractile filaments and subsequent contraction. Relaxation occurs by the removal of calcium from the cytosol by calcium transporters. It has been described that Gap junctions coordinate the contraction of individual cardiomyocytes and this force is transduced to the extracellular matrix, which coordinates the overall contraction of the heart (Harvey and Leinwand 2011). Engler *et al.,* (2008) have shown that the culturing of embryonic cardiomyocytes on a series of substrates of different elasticity has a significant effect in the transmission of contractile function and that cells in a rigid matrix are deficient in the assembly of contractile proteins and their beating frequency slows down over time (Engler *et al*., 2008). As a result, the extracellular matrix to which cardiomyocytes attach is a key factor for a highly regulated system such as the heart. In order to analyze the effect of P(3HO) on isolated cardiomyocyte contraction, fresh cardiomyocytes were seeded on P(3HO) coated cover slips and the effect of a range of frequencies on the cardiomyocyte contraction was examined. Results show that no significant differences were observed between the polymer and the control in terms of contraction and relaxation velocities expressed as 'time to peak 90%' and 'time to baseline 50%' respectively or for the amplitude of contraction (% shortening). Decreased function of individual cardiomyocyte contraction is known to lead to the deterioration of cardiac performance. Our results showed that the polymer maintains the effect of frequency on cardiomyocytes. When the frequency of the electrical impulse was increased from 5 to 0.5 seconds, the cardiomyocyte contraction decreased significantly in the control, which is the normal response in adult rat cells, but less so on the polymer. There was no significant difference in response between with and without polymer, although there was a tendency for contraction to be improved on the polymer.

As described before, calcium is a central regulator of cardiac contractibility. We have studied the effect of increasing calcium concentrations on cardiomyocyte contraction. It has been shown that an intracellular calcium increment leads to an increment in the force of contraction that results in a higher contraction amplitude until a saturation point at which no further increment in contraction occurs (Bers 2000). Our results showed that no significant differences were observed between the polymer and the control in terms of 'time to peak 90%', 'time to baseline 50%' and amplitude of contraction (% shortening). As expected, an increment in cardiomyocyte contraction was observed when the concentration of calcium was increased from 1mM to 2mM on both the polymer sample and the control, reaching a point of maximum contraction. These results showed that the polymer maintains the effect of calcium and hence the functionality of the cardiac tissue.

Our results suggest that P(3HO) supported the maintenance of the contraction of adult cardiomyocytes and hence is a promising novel material to support the heart during the regeneration process without interfering with the cardiomyocytes' performance. Hence, P(3HO) is a potential novel healthcare material that can be effectively used in myocardial tissue engineering.

4.5. Incorporation of active molecules

4.5.1. RGD immobilization

The fabrication of biodegradable constructs in tissue engineering is essential to provide a matrix for cell proliferation, migration and differentiation and to act as a support for the organ during regeneration. In addition to the biomaterial matrix, the control of cardiac cell environment can be enhanced by the design of biomaterials that provide adhesion, growth, migration or differentiation signals. Neat cardiac patches were

further functionalised via the incorporation of active factors. It has been observed that proteins that contain the Arg-Gly-Asp (RGD) sequence are recognized by several different integrins in their adhesion protein ligands (Ruoslahti 1996). In order to allow efficient host cell recruitment and adhesion, RGD motifs were immobilized on the patches. For the RGD immobilization a series of chemical reactions were carried out to incorporate active amino terminal structures on the carboxylic acid end of the P(3HO) molecule, followed by the reaction of the terminal amine with the RGD sequence. The incorporation of the amino terminal group into the P(3HO) molecule was carried out through the addition of hexaethyleneglycol-diamine to the P(3HO) carboxylic acid end. The incorporation of the hexaethyleneglycol-diamine group to the P(3HO) was confirmed by FTIR. The appearance of a band at 3400 cm-1 which corresponded to the N-H bond and the appearance of a band at 1000 cm-1 showing the presence of a C-N bond suggested the presence of the hexaethyleneglycol-diamine in the P(3HO) film. In a second step, the covalent linkage of the RGD peptide to the hexaethyleneglycol-diamine present on the P(3HO) film was studied by FTIR. Results showed the presence of a strong band at 1200 cm-1 corresponding to the C-N bonds that should be present in the RGD-P(3HO) polymer, due to the linkage of the hexaethyleneglycol-diamine with P(3HO) and with the RGD peptide. In addition, the disappearance of the band corresponding to the NH2 primary amine group further confirmed the formation of the RGD-hexaethyleneglycol-diamine- P(3HO) linkage.

With the incorporation of RGD structures in the P(3HO) cardiac patches, an increment in the hydrophilicity of the surface was expected (Lin *et al*., 1992, Lin *et al.*, 1994). As polar molecules interact better with water, an increment in the molecular hydrophilicity is usually detected when RGD motifs are immobilized. The water contact angle of the P(3HO)-RGD immobilized cardiac patches was 93.4±0.1º, whereas that of neat P(3HO)

water contact angle was 101.1±0.8 º. These results thus showed a significant decrease in the water contact angle. Hence, the expected increase in the surface hydrophilicity after the modification with RGD peptides reconfirmed the incorporation of the RGD peptide onto the P(3HO) film. Further, X-ray photoelectron spectroscopy (XPS) studies will be carried out in the future for a surface elemental analysis confirmation and tripeptide quantification.

In order to study any possible effect of the RGD immobilized peptides on the mechanical properties of the P(3HO) cardiac patches, dynamic mechanical analysis under static conditions was carried out. No differences were observed in terms of the polymer stiffness after the RGD incorporation. However, a decrease in the tensile strength was observed with the RGD immobilization. As the linkage of the RGD motifs to the surface of the P(3HO) cardiac patches were carried out through hexaethyleneglycol-diamine molecules incorporated in the polymer, differences in the mechanical properties can be attributed to the presence of these molecules which perhaps embedded themselves between the chains of the polymer, spacing them apart. In agreement with our results, previous work by other groups has shown a decrease in the tensile strength and an increment in the elongation at break when polyethylene-glycol was incorporated into cellulose acetate films as a plasticizer (Yuan *et al*., 2001). Finally, SEM images show an increment in the surface roughness after the RGD modification.

4.5.2. *VEGF incorporation*

As vascularisation is crucial in cardiac patches, VEGF was incorporated in order to assist cell growth and tissue vascularisation. Mechanical properties of the P(3HO)-VEGF cardiac patches were determined and compared with P(3HO) patches. Similar stiffness was obtained after the VEGF incorporation. However, a decrease in the tensile

strength and an increment in the elongation at break were observed with VEGF. It is possible that VEGF molecules interact with the polymer by decreasing the chains interaction and hence decreasing the tensile strength and increasing the elongation at break by stretching the chains (Wang and Wu 2005). Although an increment in the surface hydrophilicity can be expected with the incorporation of VEGF molecules, due to an increment in the surface polarity, no significant differences were observed in terms of the surface wettability after the VEGF incorporation. The reason of this observation can be related to the amount of VEGF incorporated, which was too low to have an effect on the surface wettability. SEM images show a slight increment in the surface roughness in P(3HO)-VEGF cardiac patches. Surface roughness studies should be carried out in future for a quantitative analysis.

4.5.3. In vitro cell proliferation in P(3HO) cardiac patches containing VEGF and RGD peptide

C2C12 myoblast cells were seeded on P(3HO) cardiac patches containing VEGF, P(3HO) cardiac patches containing RGD and P(3HO) cardiac patches containing both VEGF and RGD. Cell proliferation was evaluated at 24 hrs with the MTT colorimetric assay. Results showed a significant increment in the cell proliferation when VEGF or RGD were incorporated in comparison to P(3HO) patches. In terms of RGD, these results suggested that as previously reported in literature, the increased cell-polymer interactions play a pivotal role in simulating cell proliferation (Neff *et al.*, 1999). Yoon *et al.,* (2003) showed a significant increment in cell attachment when bone marrow stem cells isolated from rat were seeded on PLGA films immobilized with RGD motifs (Yoon *et al*., 2003). On the other hand, VEGF has also been shown to have a positive effect in cell proliferation. These results are in agreement with previous reports that show the presence of VEGF receptors, which were thought to be present exclusively in

endothelial cells, in a number of different cell types (Couper *et al*., 1997, Pancholi and Earle 2000, Shen *et al*., 1993). Sipahigil *et al.,* (2012) showed a significant increment in L-929 cell line proliferation with VEGF incorporation in poly(lactic-co-glycolic acid) microspheres and a direct relation was observed between VEGF concentration and % cell proliferation (Sipahigil *et al*., 2012). Additionally, our results showed a slightly higher increment in cell proliferation with VEGF than with RGD incorporation. However, from these results it is not possible to conclude if the higher effect on cell proliferation with VEGF is due to the difference in the actual effects of this factor on the cells or due to the different amounts of VEGF and RGD used in this study as the VEGF amount incorporated in each film was 2µg and in the case of the RGD, each film was reacted with a 1.5 nmoles/ml RGD solution. Finally, when both VEGF and RGD were incorporated, a synergistic effect was observed, with an increment in cell proliferation by 7 times with respect to P(3HO) patches. These results suggested that there is no interference of VEGF with RGD proteins and, hence, both can be incorporated together to achieve better conditions that mimic the extracellular matrix structure in the tissue, encouraging cell attachment and proliferation.

4.5.4. VEGF release

The drug release profiles of VEGF loaded P(3HO) cardiac patches were studied for a period of 30 days. The results obtained showed a biphasic VEGF release profile, with an initial burst release followed by controlled release. On day 30 only 50% of the drug was released from the cardiac patches indicating a sustained drug release for periods longer than 30 days, an advantage for long term release. This controlled release can be attributed to the interaction of VEGF with P(3HO) and slow degradation times of PHAs in contrast to most synthetic polymers such as PLGA, which undergoes bulk degradation (Weng *et al*., 2011). In this case, due to the short biological half-life and

the high tumorigenic potential of VEGF, a sustained release over a 30 day period is crucial to maintain a continuous stimulation, an essential feature to control the amount of released factor. This was successfully achieved with P(3HO) cardiac patches (Faranesh *et al*., 2004). In conclusion, functionalised patches containing RGD and VEGF proteins can create a perfect microenvironment that would induce vascularization and improve cell-matrix and cell-cell interactions to promote the assembly of a functional heart tissue and enhance the therapeutic effectiveness of cardiac patches.

4.6. Conclusions

The replacement of infarcted cardiac tissue with engineered extracellular matrix that provides mechanical and structural support allowing cell adhesion and proliferation remains elusive. Our studies show a novel promising biodegradable, flexible and elastomeric functional material for cardiac tissue engineering that has not been explored before. In contrast to most of the material explored so far (Table 3), P(3HO) showed similar mechanical properties to that of myocardial muscle, ideal to maintain coordinated cardiac beating allowing support of the organ during the regeneration process. This is also supported by our results that show no interference of P(3HO) with cardiomyocyte performance. Additionally, as a biodegradable material, P(3HO) degradation will allow new tissue formation with no remaining material after the regeneration process. Furthermore, this work has shown that the addition of pores, fibre structures and active molecules, such as RGD and VEGF, to the fabricated cardiac patches, are strong environmental cues that imitate the cardiac extracellular matrix structure in the tissue and enhance cell adhesion and proliferation. In this case, the

P(3HO) chemical structure allowed the successful covalent bonding of RGD tripeptides and incorporation of VEGF, that showed a favorable sustained release. This work has proven for the first time, the great distinctive features of P(3HO) for cardiac tissue engineering. Future work will involve detailed studies involving the incorporation of co-monomers into the polymer backbone to allow further fine tuning of the Poly(3-hydroxyalkanoate) properties for myocardial tissue engineering applications.

References

Balguid A, Mol A, van Marion M, Bank R, Bouten C, Baaijens F. 2009, Tailoring fiber diameter in electrospun poly(epsilon-caprolactone) scaffolds for optimal cellular infiltration in cardiovascular tissue engineering, *Tissue Eng Part A,* 15(2): 437-44.

Bers D. 2000, Calcium Fluxes Involved in Control of Cardiac Myocyte Contraction, *Circ Res,* 87: 275-281.

Boland E, Wnek G, Simpson D, Pawlowski K, Bowlin G. 2001, Tailoring tissue engineering scaffolds using electrostatic processing techniques: a study of poly(glycolic acid) electrospinning, *J Macromol Sci Pure Appl Chem,* 38(12): 1231–43.

Chen M, Patra P, Warner S, Bhowmick S. 2007, Role of fiber diameter in adhesion and proliferation of NIH 3T3 fibroblast on electrospun polycaprolactone scaffolds, *Tissue Eng*, 13(3): 579-87.

Chen Q, Harding S, Ali N, Jawad H, Boccaccini A. 2008, Cardiac tissue engineering. *Tissue Engineering Using Ceramics and Polymers,* Woodhead, CRC Pr.

Couper L, Bryant S, Eldrup-Jorgensen J, Bredenberg C, Lindner V. 1997, Vascular endothelial growth factor increases the mitogenic response to fibroblast growth factor-2 in vascular smooth muscle cells *in vivo* via expression of fms-like tyrosine kinase-1, *Circ Res*, 81: 932–939.

Drury J, Dennis R, Mooney D. 2004, The tensile properties of alginate hydrogels, *Biomaterials*, 25(16): 3187–3199.

Eichhorm S, Sampson W. 2005, Statistical geometry of pores and statistics of porous nanofibrous assemblies, *J R Soc Interface*, 2: 309–318.

Engler A, Carag-Krieger C, Johnson C, Raab M, Tang H, Speicher D, Sanger J, Sanger J and Discher D. 2008, Embryonic cardiomyocytes beat best on a matrix with heart-like elasticity: scar-like rigidity inhibits beating, *J Cell Sci*, 121: 3794–3802.

Eshraghi S, Das S. 2010, Mechanical and microstructural properties of polycaprolactone scaffolds with one-dimensional, two-dimensional, and three-dimensional orthogonally oriented porous architectures produced by selective laser sintering, *Acta Biomater*, 6(7): 2467-76.

Faranesh A, Nastley M, Perez de la Cruz C, Haller M, Laquerriere P, Leong K, McVeigh E. 2004, *In Vitro* release of Vascular Endothelial Growth Factor From Gadolinium-Doped Biodegradable Microspheres, *Magnetic Reson Med*, 51: 1265–1271.

Flemming R, Murphy C, Abrams G, Goodman S, Nealey P. 1999, Effects of synthetic micro and nano-structures surfaces on cell behaviour, *Biomaterials*, 20, 573-588.

Garlotta D. 2001, Literature review of poly(lactic acid), *J Polym Environ*, *9*(2): *63*–84.

Giraud M, Armbruster C, Carrel T, Tevaearai H. 2007, Current state of the art in myocardial tissue engineering, *Tissue Eng, 13: 1825-1836.*

Goldstein A, Zhu G, Morris G, Meszlenyi R, Mikos A. 1995, Effect of osteoblastic culture conditions on the structure of poly(DL-lactic-co-glycolic acid) foam scaffolds, *Tissue Eng*, 5: 421-433.

Guan J, Fujimoto K, Sacks M, Wagner W. 2005, Preparation and characterization of highly porous, biodegradable polyurethane scaffolds for soft tissue applications. *Biomaterials*, 26(18): 3961–3971.

Guan J, Fujimoto K, Wagner W. 2008, Elastase-Sensitive Elastomeric Scaffolds with Variable Anisotropy for Soft Tissue Engineering, *Pharm. Res.*, 25(10): 2400–2412.

Gupta V, Grande-Allen K. 2006, Effects of static and cyclic loading in regulating extracellular matrix synthesis by cardiovascular cells, *Cardiovasc Res*, 72, 375–383.

Harvey P and Leinwand L. 2011, Cellular mechanisms of cardiomyopathy, *J cell biol*, 194: 3 355-365.

Hersel U, Dahmen C, Kessler H. 2003, RGD modified polymers: biomaterials for stimulated cell adhesion and beyond, *Biomaterials*, 24: 4385–4415.

Hocking P, Marchessault R. 1994, Biopolyesters, Chemistry and Technology of Biodegradable Polymers, *London: Chapman and Hall*. Academic Pr.

Hsia H, Nair M, Mintz R, Corbett S. 2011, The fibre diameter of synthetic bioresorbable extracellular matrix influences human fibroblast morphology and fibronectin matrix assembly, *Plast Reconst Surg, 127(6): 2312–2320.*

Jawad H, Lyon A, Harding S, Ali N and Boccaccini A. 2008, Myocardial tissue engineering, *Br Med Bull,* 87: 31–47.

Jell G, Minelli C, Stevens M. 2009, Biomaterial-Related Approaches: Surface Structuring. Fundamentals of Tissue Engineering and Regenerative Medicine. Springer, 469-484.

Krupnick A, Kreisel D, Szeto W, Popma S, Rosengard B. 2001, A murine model of left ventricular tissue engineering, *J Heart Lung Transplant*, 20: 197–198.

Lampin R, Warocquier-Cle´rout, Legris C, Degrange M, Sigot-Luizard F. 1997, Correlation between substratum roughness and wettability, cell adhesion, and cell migration, *J Biomed Mater Res*, 36(1): 99-108.

Lee J, Jeong S, Bae M, Yang H, Heo D, Kim C, Alsberg E, Kwon K. 2011, Highly Porous Electrospun Nanofibers Enhanced by Ultrasonication for Improved Cellular Infiltration, *Tissue Eng Part A*, 17: 21-22.

Lebourg M, Sabater Serra R, Más Estellés J, Hernández Sánchez F, Gómez Ribelles JL, Suay Antón J. 2008, Biodegradable polycaprolactone scaffold with controlled porosity obtained by modified particle-leaching technique, *J Mater Sci Mater Med*, 19(5): 2047-53.

Lee Y, Park S, Lee W, Ko J, Kim H. 2003, MG63 osteoblastic cell adhesion to the hydrophobic surfaceprecoated with recombinant osteopontin fragments, *Biomaterials*, 24: 1059–1066.

Li D. 2011, Encyclopedia of Microfluidics and Nanofluidics, *Springer*.

Li W, Laurencin C, Caterson E, Tuan R, Ko F. 2002, Electrospun nanofibrous structure: A novel scaffold for tissue engineering, *J Biomed Mater Res*, 15;60(4): 613-21.

Lin H, Garciaecheverria C, Asakura S, Sun W, Mosher D, Cooper S. 1992, Endothelial-cell adhesion on polyurethanes containing covalently attached RGD-peptides, *Biomaterials,* 13: 905–14.

Lin H, Sun W, Mosher D, Garciaecheverria C, Schaufelberger K, Lelkes P, Cooper S. 1994, Synthesis, surface, and cell adhesion properties of polyurethanes containing covalently grafted RGD-peptides, *J Biomed. Mater Res*, 28: 329–42.

Lu X , and Chung D. 1998, A comparative study of the wettability of steel, carbon, and polyethylene fibres by water, *Cement and Concrete Research*, 28(6): 783–786.

Ma Y, Yang D, Shi W, Li S, Fan Z, Tu J, Wang W. 2012, Preparation and properties of novel poly(propylene oxide)-block-polylactide-based polyurethane foams. Polym. Eng. Sci, 53(2):343-352.

Morosco J. 2002, Conquering heart disease: a call to action, *Prev Cardiol,* 5: 31– 6.

Mosmann T. 1983, Rapid colorimetric assay for cellular growth and survival: Application to proliferation and cytotoxicity assays, *J. Immunol Methods,* 65(1–2): 55–63.

Nagueh S, Shah G, Wu Y, Torre-Amione G, King N, Lahmers S. 2004, Altered titin expression, myocardial stiffness and left ventricular function in patients with dilated cardiomyopathy, *Circulation*, 110: 155-162.

Neff J, Tresco P, Caldwell K. 1999, Surface modification for controlled studies of cell-ligand interactions, *Biomaterials,* 20(23-24): 2377-93.

Nelson T, Kaufman E, Kline J, Sokoloff L. 1981, The extraneural distribution of hydroxybutyrate, *J Neurochem*, 37: 1345-1348.

Pancholi S, Earle K. 2000, Pattern of angiogenic cytokine release from human vascular smooth muscle cells programmed by amino acid deprivation, *Cytokine,* 12: 1322–1325.

Perry E, Roth J. 2003, Cardiovascular tissue engineering: constructing living tissue cardiac valves and blood vessels using bone marrow, umbilical cord blood, and peripheral blood cells, *J Cardiovasc Nurs*, 18: 30.

Rai R, Yunos D, Boccaccini A, Knowles J, Barker I, Howdle S, Tredwell G, Keshavarz T, and Roy I. 2011, Poly-3-hydroxyoctanoate P(3HO), a Medium Chain Length Polyhydroxyalkanoate Homopolymer from *Pseudomonas mendocina*, *Biomacromolecules,* 13;12(6): 2126-2136.

Rezania A, Healy K. 2008, Biomimetic Peptide Surfaces That Regulate Adhesion, Spreading, Cytoskeletal Organization, and Mineralization of the Matrix Deposited by Osteoblast-like Cells, *Biotechnology Progress,* 15(1): 19-32.

Richert L, Vetrone F, Yi J, Zalzal S, Wuest J, RoseiF, and Nanci A. 2008, Surface Nanopatterning to Control Cell Growth, *Adv. Biomater,* 20: 8, 1488-1492.

Roeder B, Kokini K, Sturgis J, Robinson J, Voytik-Harbin S. 2002, Tensile mechanical properties of three-dimensional type I collagen extracellular matrices with varied microstructure, *J. Biomech. Eng*, 124(2): 214-22.

Ruoslahti E. 1996, RGD and othe recognitions sequences for integrins, *Ann Rev Cell Dev Bio*, 12: 697-715.

Santerre JP, Woodhouse K, Laroche G, Labow R. 2005, Understanding the biodegradation of polyurethane: From classical implants to tissue engineering materials, *Biomaterials,* 26(35): 7457-7470.

Shen H, Clauss M, Ryan J, Schmidt A, Tijburg P, Borden L, Connolly D, Stern D, Kao J. 1993, Characterization of vascular permeability factor/vascular endotelial growth factor receptors on mononuclear phagocytes, *Blood*, 81: 2767–2773.

Shin M, Ishii O, Sueda T, Vacanti J. 2004, Contractile cardiac grafts using a novel nanofibrous mesh, *Biomaterials*, 25: 3717–3723.

Silvestri A, Boffito M, Sartori S, Ciardelli G. 2013, Biomimetic Materials and Scaffolds for Myocardial Tissue Regeneration, *Macromol Biosc*, 13(8):948-1019.

Silvestri A, Sartori S, Boffito M Clara Mattu, Di Rienzo A, Boccafoschi F, Ciardelli G. 2014, Biomimetic myocardial patches fabricated with poly(E-caprolactone) and polyethylene glycol-based polyurethanes, *J Biomed Mater Res B Appl Biomater*, 102(5):1002-13.

Sipahigil O, Alarçin E, Türko lu M, Dortunç B, Karagöz H, Ülkür E, Vural M, Çapan Y. 2012, Characterization, cell proliferation and cytotoxicity evaluation of vascular endotelial growth factor loaded poly(lactic-co-glycolic acid) microspheres, *Nobel Med, 8(1): 77-82*.

Sutton M and Sharpe N. 2000, Left Ventricular Remodeling After Myocardial Infarction: Pathophysiology and Therapy, *Circulation*, 101: 2981-2988.

Wang J, Wu W. 2005, Swelling behaviors, tensile properties and thermodynamic studies of water sorption of 2-hydroxyethyl methacrylate/epoxy methacrylate copolymeric hydrogels, *Eur Polym J*, 41: 1143–1151.

Wang Y, Ruan L, Lo W, Chua H, Yu H. 2006, Construction of recombinant *Bacillus subtilis* for production of polyhydroxyalkanoates, *Appl Biochem. Biotechnolo*, 129-1332:1015-22.

Watanabe S, Shite J, Takaoka H, Shinke T, Imuro Y, Ozawa T, Otake H, Matsumoto D, Ogasawara D, Paredes O and Yokoyama M. 2006, Myocardial stiffness is an important determinant of the plasma brain natriuretic peptide concentration in patients with both diastolic and systolic heart failure, *European Heart J*, 27, 832–838.

Webb A, Yang J, Ameer G. 2004, Biodegradable polyester elastomers in tissue engineering, *Expert Opin Biol Ther*, 4(6): 801-12.

Weng Y, Wang X, Wang Y. 2011, Biodegradation behaviour of PHAs with different chemical structures under controlled composting conditions, *Polymer testing*, 30: 372-380.

Williams S, Martin D, Horowitz D, Peoples O. 1999, PHA applications: addressing the price performance issue. I. Tissue engineering, *Int J Biol Macromol*, 25: 111–121.

Yoon J, Song S, Lee D, Park T. 2003, Immobilization of cell adhesive RGD peptide onto the surface of highly porous biodegradable polymer scaffolds fabricated by gas foaming/salt leaching method, *Biomaterials*, 25: 5613-5620

Yuan J, Shang P, Wu S. 2001, Effects of Polyethylene Glycol on Morphology, Thermomechanical Properties, and Water Vapor Permeability of Cellulose Acetate–Free Films, *Pharm Technol*, 25(10): 62-74.

Zinn, M, Witholt B, and Egli T. 2001, Occurrence, synthesis andmedical application of bacterial polyhydroxyalkanoate, *Adv Drug Delivery, Rev.* 53, 5-21.

Supporting information

Poly(3-hydroxyoctanoate), a promising new material for cardiac tissue engineering

Andrea V. Bagdadi [1], Maryam Safari [1], Prachi Dubey [1], Pooja Basnett [1], Panagiotis Sofokleous [2], Eleanor Humphrey, Ian Locke [1] , Mohan Edirisinghe [2] , Cesare Terraccino, Aldo R. Boccaccini [3] , Jonathan Knowles[4,5], Sian E. Harding [6], Ipsita Roy [1]*

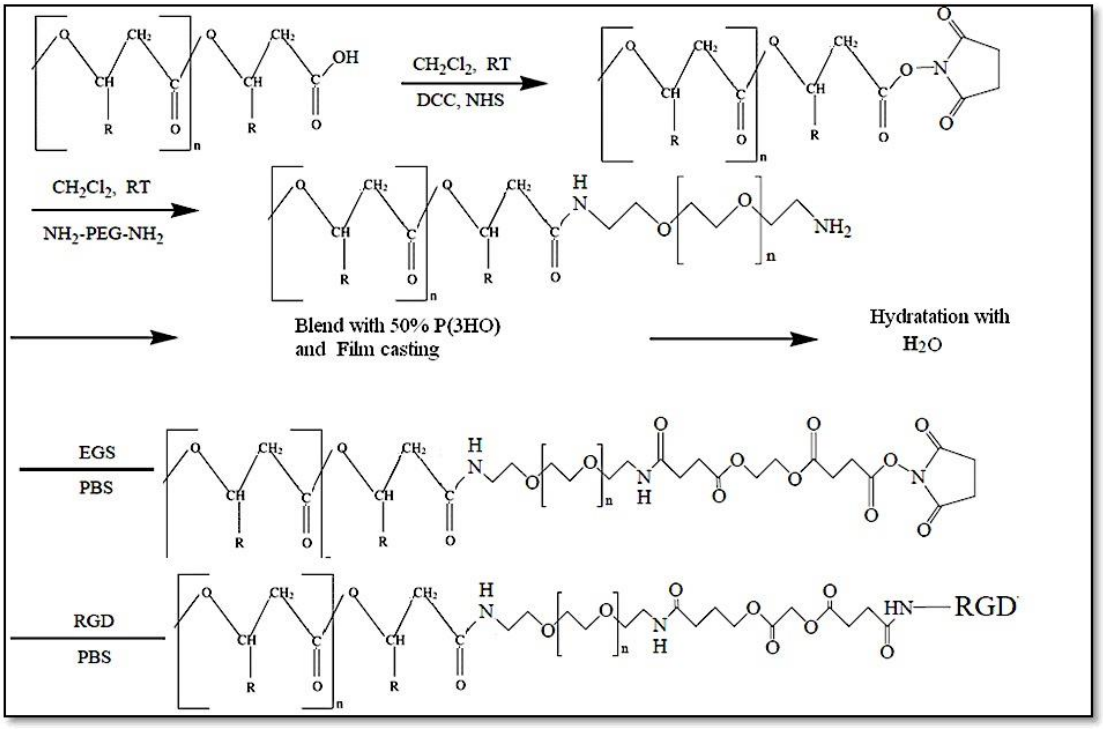

Figure S1. Synthetic scheme of the RGD peptide immobilization adapted from Yoon (2003). DCC: Dicyclohexylcarbodiimide, NHS: N-hydroxysuccinimide, EGS: ethyleneglycol-bis-succinimidylsuccinate, PBS: Phosphate buffered saline. RT: reaction carried out at room temperature.

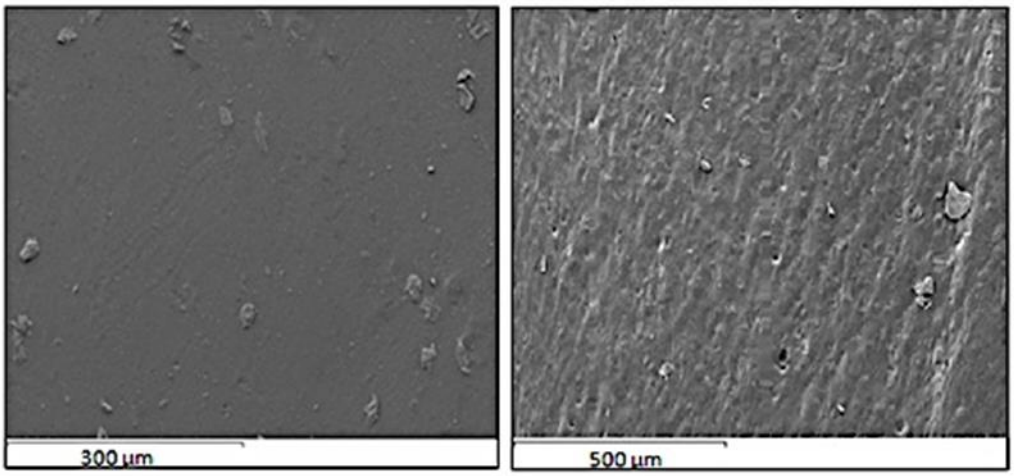

Figure S2. SEM images of A) neat and B) RGD immobilized P(3HO) patches at different magnifications showing the rough surface of the RGD modified cardiac patches compared to neat polymer constructs.

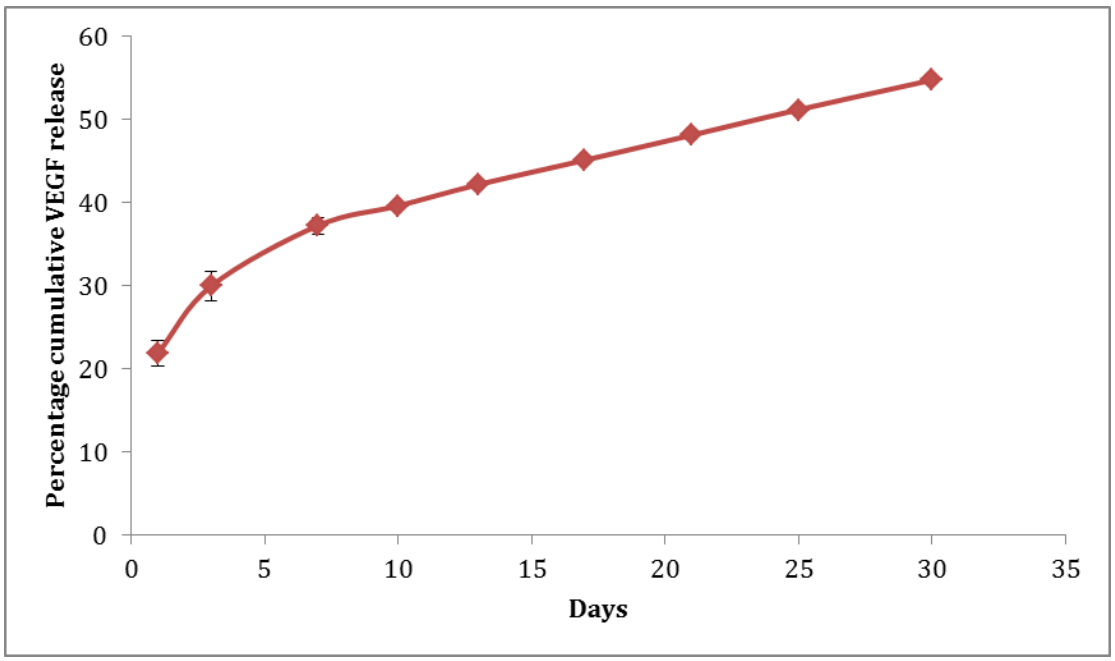

Figure S3. Release profile of VEGF from P(3HO) cardiac patches (n = 3; error bars=±SD).